2015

Computational Modelling And Surface Charachterization Of Interface In Polymer Composites By Atomic Force Microscopy

Daljeet Kumar Singh
University of Alabama at Birmingham

COMPUTATIONAL MODELLING AND SURFACE CHARACHTERIZATION OF INTERFACE IN POLYMER COMPOSITES BY ATOMIC FORCE MICROSCOPY

by

DALJEET KUMAR SINGH

UDAY VAIDYA, COMMITTEE CHAIR
AMOL VAIDYA
HAIBIN NING
VINOY THOMAS

A THESIS

Submitted to the graduate faculty of The University of Alabama At Birmingham,
in partial fulfillment of the requirements for the degree of
Master of Science

BIRMINGHAM ALABAMA

2015

COMPUTATIONAL MODELLING AND SURFACE CHARACHTERIZATION OF INTERFACE IN POLYMER COMPOSITES BY ATOMIC FORCE MICROSCOPY

DALJEET KUMAR SINGH

MATERIAL SCIENCE AND ENGINEERING

ABSTRACT

Polymer composites are used in numerous industries due to their high specific strength and high specific stiffness. Such composites have markedly different properties than both the reinforcement and the matrix. Of the several factors which govern the final property of the composite, the interface is the single most factor that influences the stress transfer mechanism from the fiber to the matrix. The interface bond strength is also influenced by the surface treatments applied to the fiber during spinning and weaving. The present study is an effort to characterize and model the fiber-matrix interface in polymer matrix composites.

Finite element models were developed to study the interfacial behavior during pull out of a single fiber in continuous fiber reinforced polymer composite. Three-dimensional (3D) unit cell cohesive damage models for the fiber/matrix interface debonding were employed to investigate effect of interface/sizing coverage on the fiber. Furthermore a 2-D Axi-symmetric model was also used to analyze sensitivity of interface stiffness, interface strength, friction coefficient, and fiber length via a parametric study. A 2-D axi-symmetric model was also used to study the shear stress distribution across the fiber-interface-matrix zone. It was determined that the force required to debond a single

fiber from a matrix is three times more if there is full distribution of the sizing on the fiber. Parametric study indicated that cohesive strength was the most influential factor in debonding. Moreover the stress distribution model showed debonding mechanism of the interface. It was observed that the interface debonded first from the matrix and remained in contact with fiber even when the fiber was completely pulled out.

Atomic force microscopy (AFM), X-ray photoelectroscopy (XPS), Fourier transform infrared spectroscopy (FTIR) and contact angle analyses were performed on seven different carbon fiber surfaces. AFM images along with surface roughness showed that roughness and mechanical properties remained same for most of the fibers, this was deduced to be due to usage of same sizing. This was also validated by FT-IR, XPS and, scanning electron microscopy (SEM) and wettability.

AFM as a surface analysis technique to quantify the characteristics of the fiber/matrix interface was implemented successfully. This study reaffirmed the belief that a combination of surface imaging tools like atomic force microscopy, x-ray photoelectron spectroscopy and finite element analysis, the interface and interphase of fiber reinforced composites can be characterized easily. Implementation of these techniques will result in easier ways to understand the fiber matrix bonding in comparison of existing methods.

ACKNOWLEDGEMENT

This thesis would not have been possible without the support of numerous individuals and institutions within The University of Alabama at Birmingham and elsewhere. First and foremost, I would like to acknowledge the tremendous support in academics and otherwise by my thesis advisor and committee chair, Dr. Uday K. Vaidya. Dr. Vaidya's guidance towards developing my research acumen has been exemplary and I am grateful to him for that. I am also thankful to my committee members- Dr. Amol Vaidya, Dr. Haibin Ning & Dr. Vinoy Thomas for their time, support and technical inputs in my research. Dr. Selvum (Brian) Pillay has been constant pillar of support and inspiration throughout my graduate studies at UAB and it has been a pleasure to work with him.

The financial support by Owens Corning Science and Technology during my graduate studies and specially this project is greatly appreciated. I would also like to thank Oak Ridge National Lab for providing us carbon fiber samples which were a crucial element in this research

I would also like to thank Dr. Jinhui Song and his PhD student Chaolong Tang for their support in conducting AFM measurements at the University of Alabama, Tuscaloosa. Dr. Michael Bozack from Auburn University has also been very helpful in conducting XPS on my samples and I am grateful to him.

Last but not the least, my fellow graduate students in the Advanced Plastics & Composites group deserve many a thanks for helping me in every possible way.

TABLE OF CONTENTS

LIST OF TABLES

LIST OF FIGURES

1. INTRODUCTION

Composite materials are a combination of two or more constituents, the fiber which is the reinforcement and the matrix, which serves as the binder and medium in which reinforcement is dispersed. The result is a material which has properties closer to the reinforcement but in a form that can be easily fabricated into various components. Reinforcement can be in the form of particulate, fiber, flake and sheet reinforcements. Matrices may be ceramic, metallic, polymeric and cementitious [1]. While the properties of the constituent fibers and matrix in a composite have been well characterized in literature; the behavior of the fiber-matrix interface remains largely unknown [2]. A large body of research has been carried out in this field, however understanding of the interface and interphase is far from complete [9].

Interface has a great influence in controlling adhesion between fiber and matrix and the resulting properties in fiber reinforced polymer composites. The interface bond strength is largely influenced by the surface treatments applied to the fiber during spinning & weaving. Sizing is a protective coating applied to the fiber surface to improve the handling of the fibers during processing and also to promote adhesion between the fiber and the matrix [3, 4]. The purpose of sizing is to insert a polymer interlayer between the fiber and the polymer matrix and to use the properties of the sizing to control the level of fiber/matrix adhesion. Sizing also has been reported to improve the wetting of fiber by

the matrix resin so as to protect its surface reactivity [5]. Moreover, the mechanical properties of composites is also compromised by presence of voids, impurities and microcracks which is concentrated in the interface region [6]. Increase in fiber surface roughness increases the total energy absorption of the interphase by improving the surface roughness and the sliding energy [7]. The poor interfacial adhesion between carbon fiber surfaces and polymer molecules caused intrinsically by hydrophobicity and chemical inertness of carbon is a long existing issue and it can be improved by modifying surface properties. It is the same for glass fibers as well, where the use of silane coupling agent is well documented but the influence of film former is yet limited. Hence a focus on development and characterization of interfaces between the fiber and the matrix is essential for the fiber manufacturing industry. With a better understanding of interface, entirely new performance standards from the reinforcement side can be achieved. This can be beneficial to various composites industries.

1.1 Motivation

There have been several techniques used by researchers to measure the fiber–matrix adhesion. These methods can be broadly classified into three categories: direct methods, indirect methods and composite lamina methods. The direct methods include the fiber pull out method, the single-fiber fragmentation method, the embedded fiber compression method, and the micro indentation method. The indirect methods for fiber matrix adhesion include variable curvature method, the slice compression test, the ball compression test, dynamic mechanical analysis, and the voltage contrast x-ray spectroscopy. The composite lamina methods include the 90^{o} transverse flexural and

tensile tests, three- and four-point shear, ±45° and edge delamination tests, the short beam shear test method, and the mode I and mode II fracture tests [8]. Typically experimental set-up for the direct test methods is very complex. Moreover data reduction and interpretation is challenging because of several factors. These include experimental data scatter, inability to always discern changes in the slopes of the recorded load-displacement plots, and the machine compliance from the recorded displacement. Pithekethly et al. [9] devised a round robin test program to evaluate different techniques to evaluate interfacial shear strength of fiber/matrix bond in composite materials. The selected tests were single fiber pull-out test, the micro bond test, the fragmentation test and the micro-indentation test. Twelve laboratories participated in this program but it was inconclusive and scatter between laboratories for a particular test was high. The researchers proposed further investigation to devise a protocol.

The traditional pull out and fragmentation tests suffer from difficulty in specimen preparation [2]. The micro bond test developed by Gaur & Miller [10] is one of the widely used single fiber-matrix interfacial bond test methods to determine interfacial shear strength IFSS [2]. However a standard procedure for micro bond is yet to be established with various researchers using different techniques to minimize the data scatter. This suggests the complexity of this technique, and the need to devise a technique to measure interfacial properties.

The strength of composite structures has historically been predicted through the mechanical testing of particular matrix/fiber reinforcement combinations. These tests include, but are not limited to, tensile testing, compression testing, shear testing, fatigue testing, or a combination thereof. It is known that many of the measured mechanical

properties of composites are governed by the quality of the adhesion between the fiber and the matrix. Without suitable interfacial interaction, proper load sharing between the fibers does not take place, resulting in a weaker material [11]. Recently, surface analysis techniques have been introduced to quantify the integrity of this fiber/matrix interface and compared to current mechanical methods. It is a common belief now that with a combination of surface imaging tools like atomic force microscopy, x-ray photoelectron spectroscopy and finite element analysis, the interface and interphase of fiber reinforced composites can be characterized accurately.

1.2 Research Objectives

This research aims to better understand the relationship between structure, properties, and functions by nanostructural design and control of surface processes. The present work explores a novel way to characterize the interfacial properties more specifically the sizing on glass & carbon fibers. It has been done in two stages: (a) finite element modeling using ABAQUS 6.13 in collaboration with Owens Corning Science & Technology, Granville, OH. Glass fiber & epoxy resin properties were used in all the analysis; (b) investigating the interphase (sizing) in terms of surface morphology and mechanical characterization using XE-70 AFM. This part of the work was done on carbon fibers provided by Oak Ridge National Laboratory (ORNL).

Objective 1: ***Formulate different computational models to study the interface and its adhesion to the fiber and matrix***

Cohesive damage analysis was used to predict the initiation and evolution of damage at the interface of the unit cell comprising of fiber and matrix. For a unit cell that consists of multiple material systems, the number of potential failure mechanisms that must be accounted for exponentially increases the complexity of the analysis. Failure mechanisms include failure at the interface, fiber breakage, matrix cracking and their interaction. Different modeling approaches within the Cohesive Zone Modelling (CZM) were employed: elements with "finite-thickness" simulate the debonding mechanism across the fiber-matrix interface, "zero-thickness" model illustrates the interface failure between the fiber & the matrix. This was achieved using two different models- (a) model in which the interface was modeled as zero thickness and adhesive properties were used to study the interface failure mechanism; and (b) a very small thickness was provided in the finite thickness model. Parametric studies were also conducted to study the most influential factors affecting strength of the fiber matrix unit cell.

Objective 2: ***Surface characterization using AFM to quantify different interfaces***

To better understand the effect of sizing on the interphase between fiber and resin, this work investigates the nanoscale nature of the sizing in terms of roughness, elastic modulus and hardness of the sizing on carbon fibers. Six types of carbon fibers were selected with unknown sizing. Single fiber fragments of these fibers were scanned in an Atomic Force Microscope (AFM) to measure the mechanical properties. Surface topography and phase imaging was also conducted. While surface analysis for fibers has been done in the past [5, 7, 12, 13], mechanical properties of the sizing are relatively

unknown. Over recent years, a significant amount of effort has been spent on estimation of mechanical properties of soft biological samples using FD spectroscopy [14-16], a similar attempt is made here using FD spectroscopy to calculate Young's modulus, hardness and indentation depth for different sizings on carbon fiber filaments.

2. LITERATURE REVIEW

2.1 Glass fiber and characterization of its interface

Glass fiber reinforced polymer matrix composite materials are used in numerous applications ranging from automotive to construction to aerospace and defense. The mechanical behavior of continuous fiber reinforced composite is dependent on its constituent properties- fiber, matrix and the fiber/matrix interface [17]. While the properties of the constituent fibers and matrix in a composite have been well characterized in literature; the behavior of the fiber-matrix interface or the sizing remains largely unknown [2].

The interface bond strength is largely influenced by the surface treatments applied to the fiber during spinning & weaving. Sizing is a protective coating applied to the fiber surface to improve the handling of the fibers during processing and also to promote adhesion between the fiber and the matrix [3, 4]. The sizing comprises of several components of which the film former and the coupling agents are of primary interest. The function of the film former is to provide protection to the fiber while the coupling agent provides the fiber-matrix bond strength. An interface forms when the sizing reacts to the fiber and the matrix during processing and consolidation. While the entire region between the fiber & matrix is referred to as interface, it should be noted that the fiber –sizing region is referred to as the ‘interface ‘while the sizing-matrix region is referred to as the

'interphase' because of the chemical reactions that occur between the sizing and resin due to consolidation and curing [2]. Sizing plays an important role in case of glass fibers, this has been described in detail by Thomason and Adzima [4]. They demonstrated that with optimum levels of silane and a combination of 3-amino-propyltriehoxysilane (APS), the tensile strength of the composite depends on the APS levels.

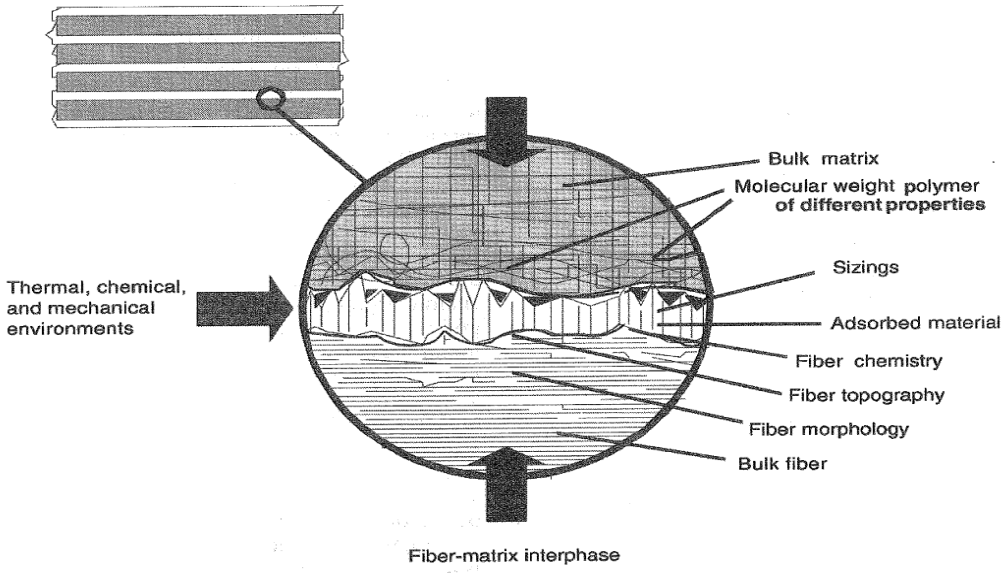

Figure 1: Schematic diagram of the fiber-matrix interphase and some of the factors that contribute to its formation [8]

The interphase includes not only a 2D area of contact (interface) between the fiber and the matrix, but also a finitely thick region extending on both sides of the interface in both the fiber and matrix [18]. Ever since polymer composites have gained prominence in numerous industries, researchers have tried to study the interphase in terms of its thickness. Microscopic FTIR spectroscopy was used by Ikuta et al. [19] on thin-sliced samples. Scanning of these samples and calculating difference in spectra for glass and vinyl ester resulted in evaluation of interphase thickness of 80 μm. Interphase thickness was also investigated using nanoindentation and nanoscratch method which is more

reliable by Hodzic et al. [20]. An interphase thickness of 2 μm & 6 μm for glass/polyester and Glass/phenolic composite system was measured respectively. Furthermore, a range of interphase thickness (0.8 to 1.5 μm) was measured by Kim et al. [21]. They attributed this range due to difference in concentration of silane coupling. Nanoindentation and nanoscratch was also employed in this research. It has also been reported in early literature that Raman and NMR spectroscopy can be used to characterize the chemical aspects of the interphase [19]. It is widely known now that an interphase is formed on silane coated glass fibers when they come in contact with curing resin. This liquid before the cross linking contains a mixture of polymers and oligomers and therefore is similar to a polymer blend [22].

Thomason [23] demonstrated that interfacial strength of composites is dependent on the nature of glass fiber coating and on the type of curing agent in the resin formulation. Mader et al. [24] demonstrated that with change in change in formulation of the film former and modification of the polypropylene resin, they could achieve better interfacial properties for composites. This was attributed to change in acid-base properties of the glass fiber by interaction of the film formers. Hence, optimal interfacial properties could only be achieved if the sizing formulation is designed so as to control chemical bonding with fiber surface texture [7]. Generally speaking glass fiber sizings comprise of silane coupling agents, film former, emulsifier, anti-foam agents and anti-static agents. Some of the patent literature [25-27] by fiber glass manufacturers gives us some basic understanding on sizing formulations.

Similar to fiber glass reinforced with thermosets, glass fibers reinforced with thermoplastics also show the same dependency on interfacial properties as far as

interfacial properties are concerned. Scholtens et al [28] conducted their study with glass fiber and polypropylene (PP) and rubber-modified styrene-co-maleic anhydride. Some of the main findings were immiscibility of the film former into the matrix and indiffusability into the bulk resin. They also concluded that ILSS values for composite wherein matrix compatible film formers with optimum ratio of silane coupling agent increased by more than 100% in comparison with incompatible film formers. Moreover, Gao et al [29] have concluded in their research that commercial sizing packages include other additives which improve the energy absorption property. This was revealed when a comparative study was conducted between model sizing systems with only silane coupling agents and silica and commercially available sizing packages. Moreover, they also concluded that addition of colloidal silica within the sizing increases the surface roughness by threefold. This sizing formulation was also instrumental in greater interfacial shear strength (IFSS) values for the composites using this system.

2.2 Carbon Fiber and Characterization of its Interface

A carbon fiber is a long, thin strand of material about 0.0002-0.0004 in (0.005-0.010 mm) in diameter and composed mostly of carbon atoms. These atoms are bonded together in crystals which are aligned parallel to the axis of the fiber. The result is extremely strong fibers. Several carbon fibers are twisted together to form a yarn, which may be used by itself or woven into a fabric. The raw material used to make carbon fiber is called the precursor. Around 90% of the carbon fibers produced are made from polyacrylonitrile (PAN) and the remaining 10% are made from rayon or petroleum pitch [30]. All of these materials are organic polymers, characterized by long strings of

molecules bound together by carbon atoms. The exact composition of each precursor varies from one company to another and is generally considered a trade secret [30].

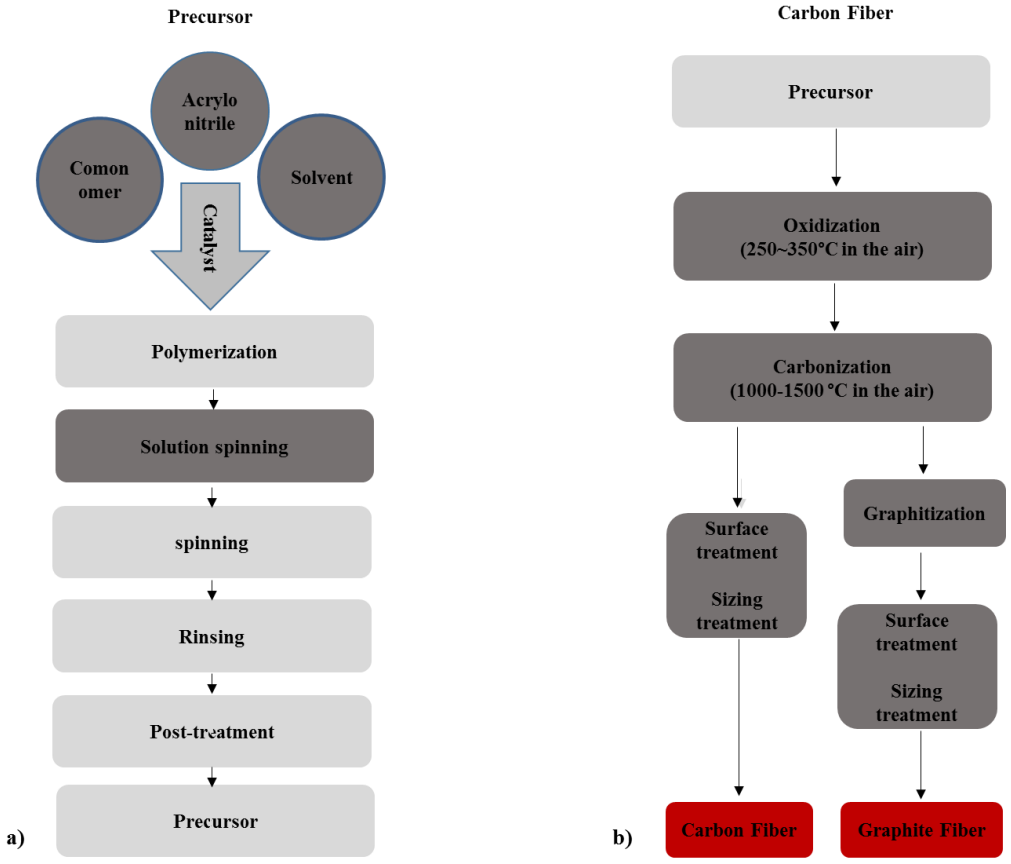

Figure 2 Schematic of carbon fiber manufacturing process. Adapted from [31]

Stabilization of polyacrylonitrile (PAN) into ring structure and high temperature condensation of the resultant into two dimensional graphite-like structure are two of the major steps in conversion of PAN to carbon fibers [32]. It is also worth noting that graphitic crystallites which are formed during the conversion of PAN decide the properties of the carbon fiber. These crystallite is composed of layers of graphite arranged turbostratically into a layered structure [33]. Time temperature conditions of the fiber determines its final property- longer residence time & graphitization temperature

makes the crystallites go bigger and the result is high modulus carbon fiber on the other hand low modulus fibers are produced at low temperature wherein graphitic basal planes are less [33].

Carbon fiber reinforced composites are widely used in aerospace, enginery, marine and automobile industries due to their outstanding properties such as high specific strength and stiffness, lower density and flexible design [1]. Carbon also potential as a biomaterial due to its biocompatibility and its lower density, mostly the form used is graphite since it is not highly ordered [34]. The demand for carbon composites can grow even more if interfacial properties could be enhanced which directly affects the mechanical property of the composites. A large body of research has been conducted over recent years [5, 12, 13, 35] to understand interface & interphase and their impact on final properties of carbon fiber reinforced composites. Composites used for structural application require a very strong fiber/matrix interface whereas those used for impact performance and/or damage tolerance require an interphase with high energy absorbing capability [7]. To achieve better impact toughness a flexible interface is thought to be more beneficial [36]. Progress has been made in the control of surface size, size distribution, composition, and assembly to achieve reproducibility and scalability of material synthesis and consolidation process. [12]

Significant attention has been devoted to comprehensively characterize the chemistry and physics of carbon [37]. As is known, the main constituent of carbon fiber is carbon itself. Earlier it was understood that the only other surface constituent was oxygen however with recent advancements in the field of surface spectroscopic tools the knowledge has widened.

With the advent of Auger and XPS equipment, researchers believe that in addition to carbon and oxygen, other elements including nitrogen, Sulphur, silicon and trace metals can be present on the fiber surface and from external environment like the oven [33]. However it is also been observed that these constituents decrease if the graphitization temperature is increased [33].

Commercially available carbon fibers are normally coated by a sizing layer on the surface which usually presents as solution or emulsion consisting of polymeric components [38]. Fiber handling, protection and wettability are some of the sizing functions which are very crucial for the end properties of Carbon fiber reinforced composites. The amount of sizing varies between 0.5-1.5 wt. % of the fiber depending on the fiber type and its intended purpose [33]. Cao et al [39] investigated the use of Thermoplastic polyimide GCPI^{TM} (heat resistant) in the formulation of sizing agent for epoxy and PAN carbon fibers. By comparing sized and unsized fibers, the researchers concluded that interfacial shear strength improved by 97% and the wear resistance also improved. On the contrary Dilsiz [5] showed that carbon fibers sized with polyimide and polyurethane(PU) in epoxy matrix have lower interfacial shear strength than unsized fibers by single fiber fragmentation test, which can be due to changes in the surface chemistry.

Even though in recent years we have developed super reinforcements such as carbon nanotubes with Young's modulus ranging from 1.0-1.5 TPa and tensile strength from 30 to 60 GPa, their use with functional polymers is still debatable due to intricacies involved in dispersion, adhesion and morphology issues [12]. The surface chemistry for carbon fibers also differs if we compare fibers in terms of their strength and modulus

properties. High modulus (HM) carbon fibers (Young's modulus around 540 GPa) have been found to be more chemically inactive than high tensile strength fibers [40]. This inert behavior presents an adverse effect as it hinders adhesion to the epoxy matrix, hence the interfacial shear strength for HM Fibers is only around 50-70 MPa [41]. Various researchers have tried to achieve better surface behavior by using plasma coating, plasma activated chemical vapor deposition both in traditional fiber-composites and metal fiber composites [42, 43]. The most important aspect in surface treatment is to make the carbon fiber surface more reactive in order to counter the inertness of carbon. Nitric acid, potassium permanganate, chromic acid, and sodium hypochlorite are some of the chemicals used to make the carbon fiber surface more wettable [34]. Fiber surface roughness is believed to be one of the most important factors in improving the bond between the fiber & the matrix [40, 44]. Fiber wettability also needs to be taken under consideration along with roughness [13]. In defining the solid surface property of carbon fiber it is very important to understand the surface energy which is divided into dispersive and polar components. Dai et al. [38] used Inverse Gas Chromatography (IGC) on sized and unsized carbon fibers along with epoxy resin to measure the surface energies and concluded that desizing reduced the percentage of activated carbon atoms especially the polar groups which led to decrease in polar component of the surface energy. The acid and base parameters measured by Dai et al. further revealed that removing the sizing decreased the acid parameter which was attributed to increase in carbonyl group content. Their work also presented a contradiction in respect to other literature available. It was found that with sizing removal, the interfacial shear strength (IFSS) increased by 38% ,

this was attributed to only physical interactions without any chemical interactions once there was no sizing involved.

2.3 COMPUTATIONAL MODELING USING ABAQUS

Analytical and numerical models are preferred due to their time and cost saving potential. Theoretical models have been very popular to understand the load displacement behavior when a single fiber is pulled out from the matrix [45-47]. Stang and Shah [46] developed a closed form solution to calculate the ultimate fiber tensile strength when debonding failure occurred. Interfacial friction as measure of debonding behavior was predicted using a simple shear lag model by Gao et.al [47]. Moreover they modeled the force-displacement behavior using interface toughness and friction as parameters. Residual clamping stresses and Poisson contraction for the fiber were taken in consideration to analyze the stresses required to debond the interface by Hsueh [45].

Finite element models have also gained a lot of popularity over the years due to technical advancement capabilities available in commercial packages. Sun and Lin [48] analyzed the interfacial properties through parametric studies in which they varied the stiffness for fiber and matrix coupled with irregular fiber cross-sections. Shear stress distribution across the interface and its effect on debonding was studied in detail by Wei et al [49]. Cohesive zone modelling has emerged as a great tool in formulating simulation models to study the interface. Dugdale [50] and [51] were the pioneers in implementing cohesive damage modelling which relies on crack initiation and its propagation. Chandra [52] in study of interfacial fracture toughness presented a detailed discussion on cohesive damage model and its reliance on traction separation laws to simulate crack initiation.

The failure of the interface is conventionally studied using a linear elastic fracture mechanics approach. In this approach, the local crack tip field is characterized using parameters such as stress intensity factors (K_I, K_{II}, and K_{III}) and strain energy release rates (G_I, G_{II}, G_{III}). These parameters determine the initiation of the crack growth. However, traditional fracture mechanics approaches assume the existence of a sharp crack with stress levels locally approaching infinity. These crack tips are also known as singular crack tip. Moreover, in reality these crack tips do not exist in the fiber matrix interface hence Cohesive Zone Modeling (CZM) is an alternative to traditional fracture mechanics approaches and this method is used for finite element analyses.

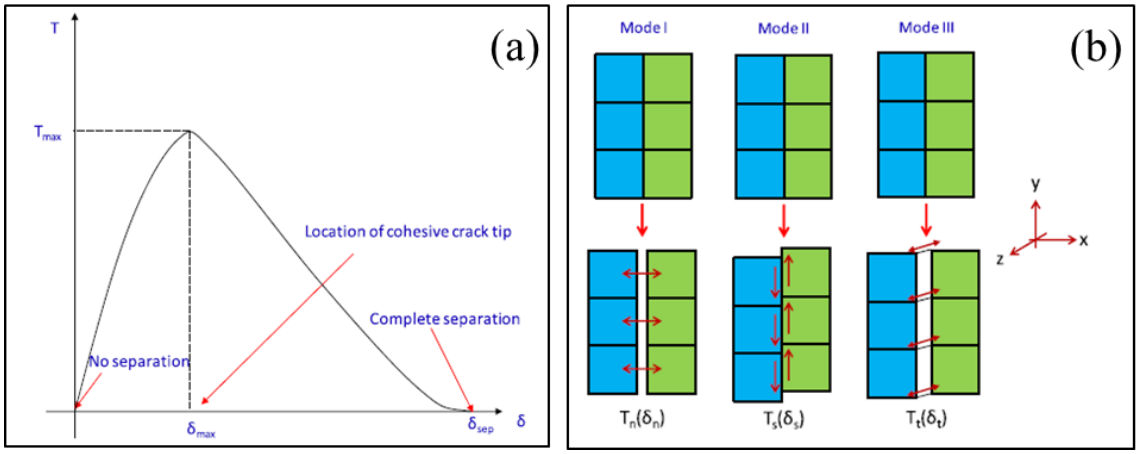

Figure 3: (a) represents the typical traction separation behavior when a fiber is pulled out from the matrix [53] and, (b) represents the traction separations for different fracture modes. Mode II fracture mode has been used for our analysis purposes [54]

Bilinear cohesive law is implemented in our modelling, see equation 1 which reduces the artificial compliance inherent in CZ model. τ_{is} , is the average interfacial shear stress and δ is the relative tangential displacement. The traction across the interface

increases and reaches to a peak value, then decreases and eventually vanishes permitting a complete decohesion.

$$\tau_{is} = K\delta \quad 0 \leq \delta \leq \delta_s \tag{1}$$

Commercial finite element code (ABAQUS ver. 6.13) has been used to model the cohesive zone in the fiber/interface debonding and/or pull out. The relation between traction stress and separation is given by equation 2,

$$\begin{Bmatrix} T_n \\ T_s \\ T_t \end{Bmatrix} = \begin{bmatrix} K_{nn} & K_{ns} & K_{nt} \\ sym & K_{ss} & K_{st} \\ sym & sym & K_{tt} \end{bmatrix} \begin{Bmatrix} \delta_n \\ \delta_s \\ \delta_t \end{Bmatrix} = K\delta \tag{2}$$

where T_n is the traction stress in the normal direction, T_s, T_t are traction stresses in the first shear and the second shear directions respectively, K is the normal stiffness matrix, δ_n, δ_s & δ_t are separations in normal, first and second shear directions respectively. The elastic stiffness & the cohesive strength would be obtained from experiments. The maximum stress criteria is used to predict damage initiation, given by equation 3.

$$max\left\{\frac{T_n}{T_n^p}, \frac{T_s}{T_s^p}, \frac{T_t}{T_t^p}\right\} = 1 \tag{3}$$

T_n^p, T_s^p, T_t^p , signify the peak values for traction stresses in respective directions. Damage evolution law describes the rate at which the cohesive stiffness is degraded once the corresponding initiation criteria is reached. A scalar damage variable, D, represents the

overall damage at the contact point which is represented as below. The value of D ranges from 0 to 1. Refer equation 4.

$$T_s = (1 - D)T_s \quad (4)$$

2.4 Surface Characterization using AFM

The atomic force microscope (AFM) was first introduced in 1986 as a new instrument for examining the surface of insulated crystals [55]. Although it was implied from the beginning that it had the capability of resolving single atoms, strong evidence for atomic resolution did not appear until 1993 [55]. The AFM belongs to the family of scanning probe microscopes (SPM). SPMs are designed to measure local properties, such as height, friction, magnetism, with a probe. To acquire an image, the AFM probe scans a small area of the sample, measuring the local property simultaneously.

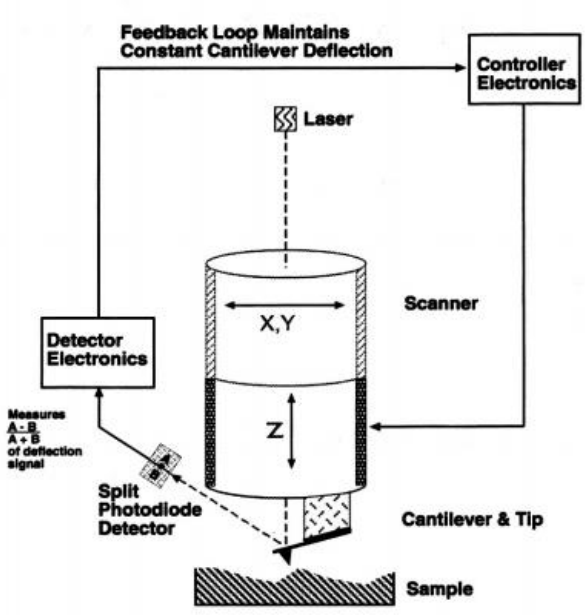

Figure 4 Schematic of Atomic Force Microscopy [56]

AFM is a surface analysis technique capable of imaging the topography and morphology changes of a specimen surface. Instead of monitoring changes in tunneling current like STM, AFM profiles a surface by utilizing the inter-atomic forces between an atomically sharp tip and the sample surface in either an ultra-high vacuum environment or under ambient conditions. As the tip approaches the surface, forces are exerted on the probe. This causes a small deflection on the attached cantilever beam that is proportional to the surface features on the specimen. A laser photodiode detector, as seen in Figure 4, can then easily measure this deflection. In addition to the topographical information that is obtained, the AFM also calculates the force exerted on the probe tip by the use of the cantilever spring constant [15]. There are three modes of the atomic force microscope: contact mode, non-contact mode, and tapping mode. The most common (and simplest) mode is the contact mode where the tip runs across the surface and is actually brought into contact with the surface and is deflected by defects in the specimen [57].

Table 1: Advantages and disadvantages of tapping mode AFM from Digital Instruments Scanning Probe Microscopy Training Notebook [56]

Advantages:
• Higher lateral resolution on most samples (1 nm to 5 nm). • Lower forces and less damage to soft samples imaged in air • Lateral forces are virtually eliminated, so there is no scraping.
Disadvantages:
• Slightly slower scan speed than contact mode AFM

The AFM is increasingly becoming a useful tool to study the topography, phase and mechanical properties of solid materials. The cantilever of the microscope acts as a sensor, probing the local interaction between the tip and the sample. The probe-sample interactions are monitored depicting the maps of the material topography as well as those properties such as mechanical, electrical, and magnetic properties. Besides topography information, phase imaging is a powerful tool that provides nanometer-scale information often not revealed by other microscopy techniques.

The causes of difference in pixels in AFM topography (also called height) and phase images can be complex. Height micrographs are recorded by maintaining a constant oscillation amplitude and recording the required vertical position of the scanner head at each (x, y) data point. A brighter area in height image is interpreted as higher than a darker area. However, it is reported that the contrast in height images of some heterogeneous materials varied or even reversed depending on the parameters such as free oscillation amplitude of the cantilever (A_0) and the set-point amplitude (A_{sp}). [58]

The difference in phase images is even more complex. Phase lag is very sensitive to variations in material properties such as adhesion and viscoelasticity. The difficulty in interpreting phase images results from the variety of parameters that influence the signal: the surface chemistry, instrument parameters, and probe tip quality [59]. Rath et al. [58] observed reversal of phase contrast upon changing parameters of A_0 and A_{sp}. Chen et al. [60] reported that the principal factor to determine phase contrast is the attractive or repulsive probe-sample interactions rather than variations in energy dissipation due to shifting probe-sample interactions.

3. OBJECTIVE I: COMPUTATIONAL MODELLING

3.1 Effect of continuous and discontinuous bonding between the fiber and matrix

A 3 D finite element model of fiber pull-out specimen was generated using a cohesive damage modeling approach. The Finite Element model of unit cell and the boundary condition is shown in Fig. 5. The radius of the fiber was 7.5μm and the fiber was encased in a square matrix which was 18.8 μm. The dimension of the matrix was based on a fiber volume fraction of 60%. Both the fiber and the matrix were modeled using 3D first-order (linear) hexahedron elements with incompatible modes (C3D8I) in ABAQUS which is an improved version of C3D8 element. More details about this type of element are available from ref [53]. The interface was modeled with zero thickness. In this model, the Young's modulus value for the interface was assumed to be equal to the matrix properties. However, the interfacial shear strength or the strength of the interface was taken from [61] which is 25 MPa. This value was measured by single fiber fragmentation test wherein a single fiber was embedded in an epoxy matrix by Kumar [61] who studied the effect of sizing on interfacial strength properties. The material and input parameters are summarized in Table 1. The contact behavior of the fiber/matrix interface was modeled as discussed earlier in chapter 2 using surface based cohesive behavior, which is similar to the cohesive element approach. This is a preferred approach when the interface or the adhesive layer is very thin [53]. A displacement controlled load

of 0.1 mm was applied atthe free end of the fiber. The reason for imposing displacement on the fiber; it results in a more gradual failure process than a similar loading using applied forces [62]. A similar approach was used by Bhemareddy et al. [63] in their finite element model for debonding of silicon carbide fiber (SiC_f) embedded in silicon carbide matrix (SiC).

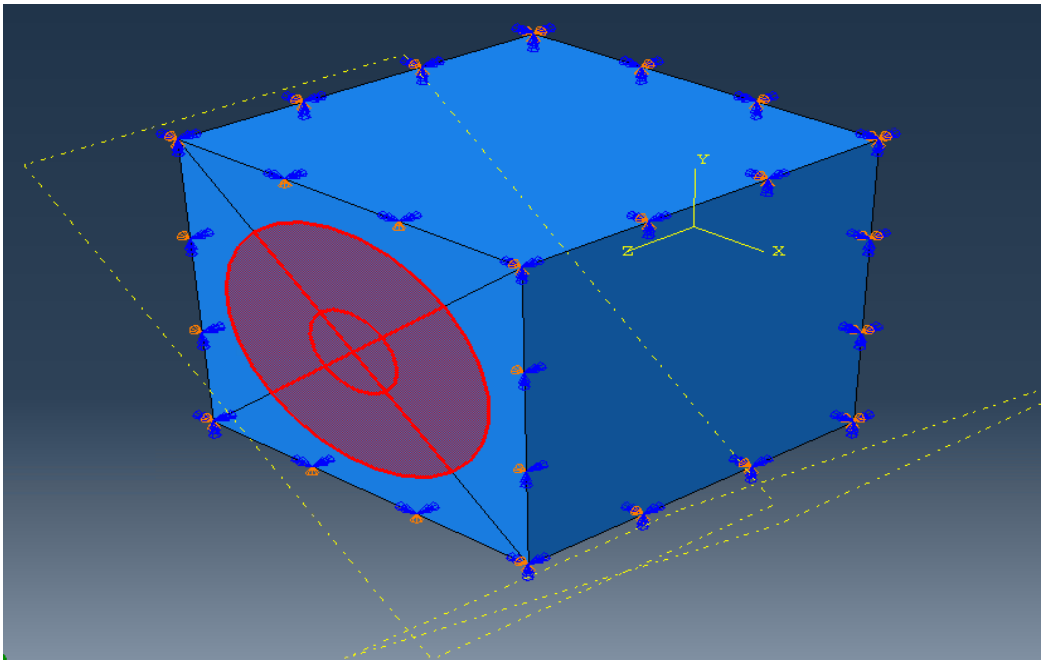

Figure 5: 3-D unit cell model where the purple circle indicates the fiber and the square represents the matrix within which the fiber is enclosed. The boundary conditions are also shown here

Two cases were studied with this model to understand the effect of sizing coverage on the fiber. In one case the complete surface of the fiber is bonded to the matrix while in the second case only half the surface of the fiber is bonded to the matrix. This simulates the situation where only half of the fiber has been coated with sizing while

the other half is uncoated. This is very close to the real-life situation wherein a typical sizing applicator operates on at least two bundle of fibers. Each bundle of fibers travels from a bushing above this applicator down to a winder below [3]. Due to the nature of this process uneven sizing is deposited on the fiber surface.

The stresses on the matrix region for discontinuous part (shown in 6b) are one magnitude lower than the one for continuous part. This can be attributed to the fact that less force is required in case of discontinuous model. The force required to pull out the fiber from the matrix increasing for continuous model was 0.06 N while it was only 0.015 N for discontinuous part. This is represented in Fig. 6(c).

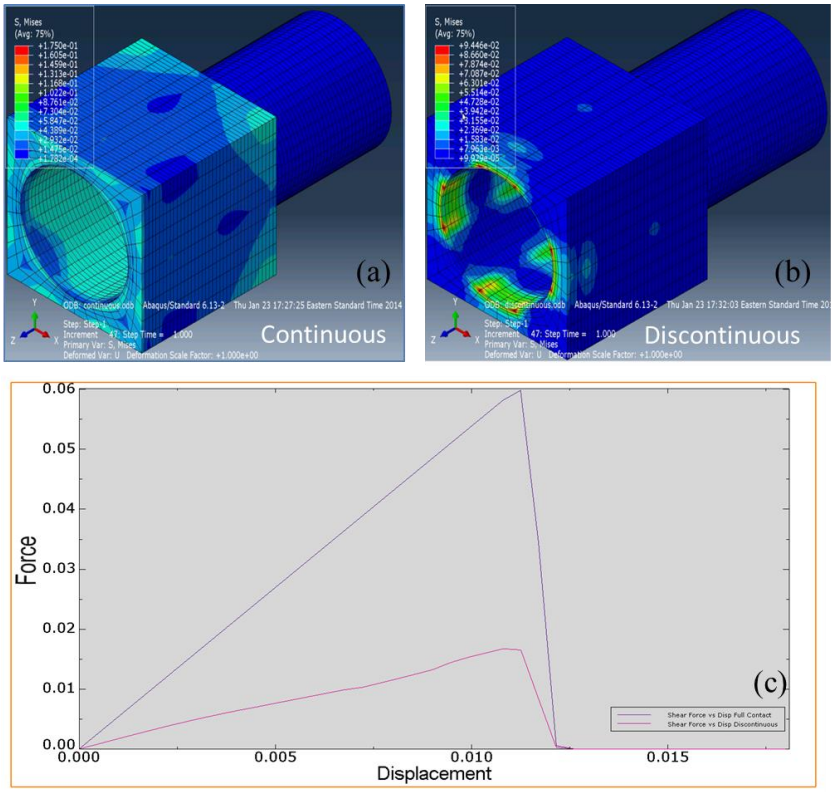

Figure 6 (a) Stress plot for continuous interface coating on the fiber,(b) Stress plot for discontinuous interface coating on the fiber, and (c) Force-displacement plot for the simulated fiber pull out where force is measured in (N) and displacement in (mm)

Table 2 material properties used in 3D model

Material	Modulus (GPa)	Tensile Strength (MPa)	Coefficient of Friction (Static & Dynamic)	Poisson's Ratio
E-Glass Fiber	72	-		0.2
Epoxy Matrix	4.2	-		0.34
Interface (Cohesive Zone)	4.2	25	1 & 0.9	-

The 3D model simulates the situation when only half of the fiber is bonded to the matrix, and it has the potential of near-accurately predicting the load displacement behavior when a single fiber is debonded from an encased matrix. With larger data sets available from experimental results in the future, this model can be used to capture details which otherwise are difficult to study using experimental or analytical methods. Furthermore, it can be used in the fiber manufacturing industry to characterize different fiber surfaces.

3.2 Parametric study to understand influential factors in fiber matrix adhesion

A parametric study was undertaken on a 2-D Axi-symmetric model to understand the influential factors affecting the fiber-matrix adhesion. Load-displacement behavior predicted by changes in these factors were recorded and compared with each other. The radius of the fiber is 7.5μm and that of the matrix was 1.5 mm. Both the fiber and the matrix were modeled using four node bilinear axi-symmetric quadrilateral elements with reduced integration (CAX4R). CZM was used for this model. A displacement controlled load of 0.1 mm is applied on the free end of the fiber. The factors studied are: (a)

coefficient of friction (static & dynamic), (b) cohesive stiffness of the interface, (c) cohesive strength of the interface, (d) fiber embedded length

Effect of coefficient of friction

The parameter- coefficient of friction primarily comes into play only after complete debond has taken place. Figure 6 shows the load displacement plots for the finite element models with varying coefficient of friction. Four different sets of static & dynamic coefficient of friction were used in the parametric study. They were: (1 & 0.9), (0.8 & 0.4), (0.4 & 0.3), (0.1 & 0.05) respectively.

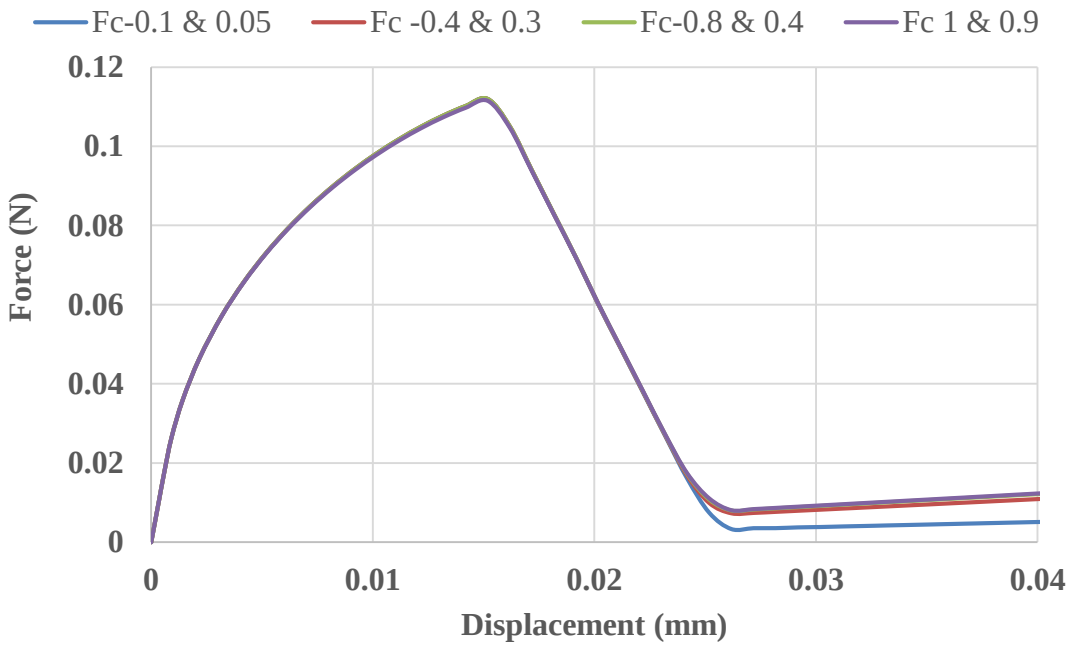

Figure 7 Force displacement curve for varying coefficient of friction

The figure 7 above is a magnified version and hence the Force-Displacement curve's non-linearity is exaggerated. However, the nature of the curve is non-linear. This could be due to effects of coefficients of thermal expansion and residual stresses on the

fiber which have not been accounted for in this model. Nevertheless, finite element models generated by various researchers [2],[29],[64] have the same trends associated with the force displacement curve.

Table 3 Baseline material properties used in 2D axisymmetric model

Material	Modulus (GPa)	Tensile Strength (MPa)	Coefficient of Friction (Static & Dynamic)	Poisson's Ratio
E-Glass Fiber	72	-		0.2
Epoxy Matrix	4.2	-		0.34
Interface (Cohesive Zone)	4.2	25	1 & 0.9	-

Effect of Cohesive Stiffness of the interface

The elastic modulus/stiffness of the interface was provided as an input property in the cohesive behavior for the interface in ABAQUS. The basic assumption here was that the interface would behave similar to the matrix, hence properties of epoxy matrix were considered as the baseline. The interface stiffness was varied from 10% of the matrix stiffness to 1000% of the matrix stiffness. As reported in Table 3, the elastic modulus for the epoxy matrix and the interface was considered to be 4200 MPa. Fig 7 shows the load displacement behavior for varying modulus of the interface. It was noticed that the peak force required for debond does not change even when the modulus of the interface is as low as 420 MPa. Also, higher the stiffness of the interface lesser is the displacement (complete separation). Furthermore, it was seen that for very low interface modulus (420 MPa) the evolution of crack length is much higher when compared to other cases. This is along the expected lines, since the interface is too weak.

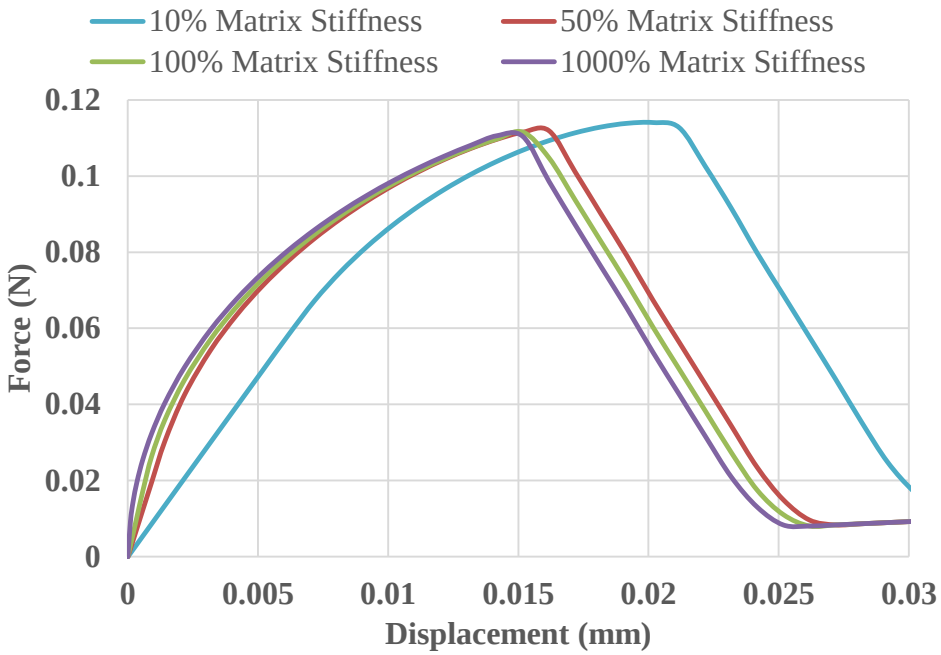

Figure 8 Force displacement curve for varying interface stiffness

Effect of Cohesive strength of the Interface

The strength of the interface was varied starting from 1 MPa to 10 MPa keeping all the other variables at the baseline configurations. It can be clearly seen from Fig. 8 that interfacial strength would directly affect the maximum load at which interface fails. The peak load is almost proportional to the strength of the interface. It is also worth noting that at higher strength, ductile behavior of the interface is seen. In other words, the crack has initiated but as the bonding strength is too high the crack evolution does not take place and debonding is delayed.

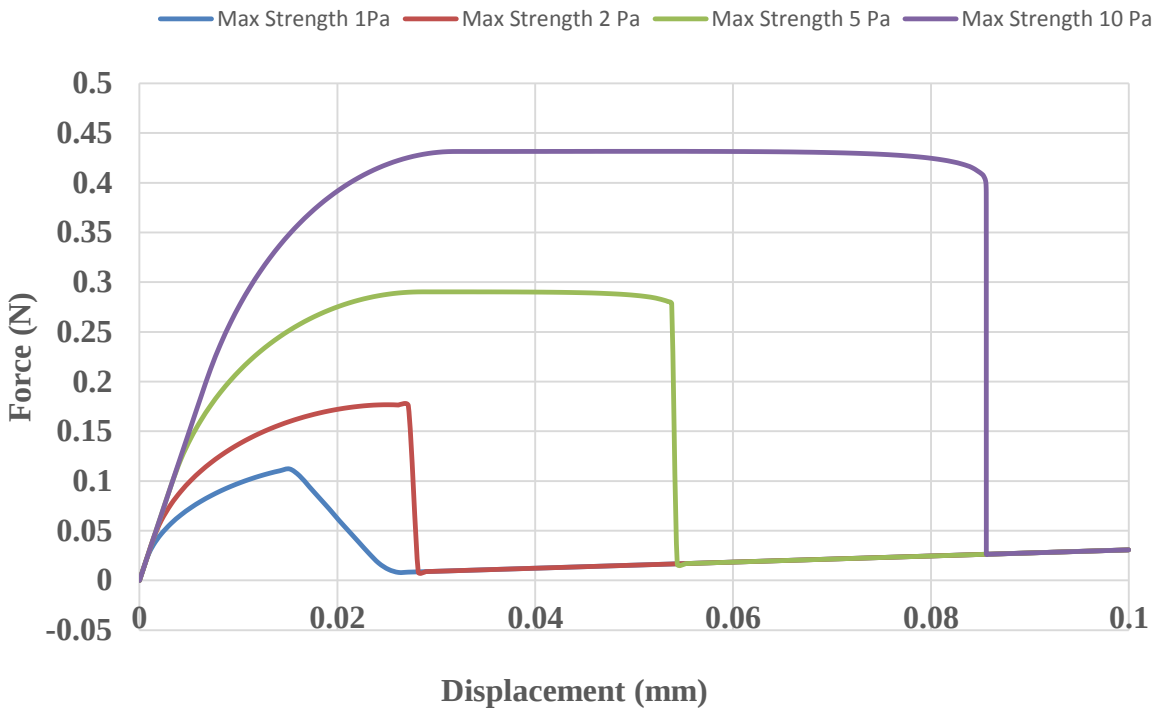

Figure 9 Force displacement curve for varying cohesive strength

Effect of embedded fiber length

The effect of fiber embedded length is more pronounced in terms of the maximum separation achieved. Three different fiber lengths (3mm, 6mm & 9mm) were used in the parametric study and the respective load displacement chart is illustrated in Fig. 8.

As the fiber length was increased, it was observed that the fiber-matrix model became more compliant and delayed debonding is observed. A similar observation was observed by Sockalingam et al. [65] when they developed a finite element model of microdroplet test method. As discussed in chapter 2, microdroplet test is one of the best techniques available to study the interfacial properties between a fiber-matrix composites. This can

be attributed to the fact that fiber takes more of the load when it is pulled out of the matrix.

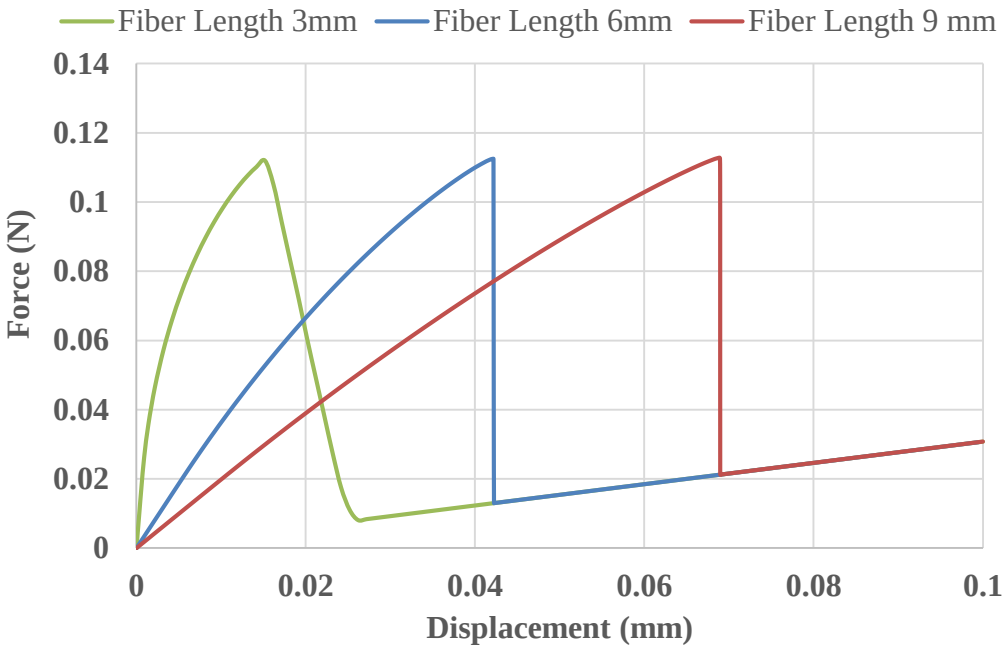

Figure 10 Force displacement curve for varying fiber length

3.3 Stress distribution at debonding between the fiber, interface and the matrix

Shear stress distribution across the interface during the debonding stage is an important indicator of performance of the interface and adhesion within the fiber/matrix in general. To investigate this effect a 2-D axi-symmetric model was created where the interface was given a thickness of 0.001 mm, the fiber diameter was 0.007 mm and the matrix was 1.5 mm. This is shown in Fig 10. Furthermore, the interface was divided into three sections and each had its own isotropic material property assigned. The three sections were: (a) interface close to the fiber which was assigned fiber property (b)

Interface in the middle which was assigned the average material property of fiber & resin (c) interface closer to resin which is matrix dominated. The representation of the model is shown in Fig. 10. The details of the input properties used in ABAQUS are provided in Table 4. The assumption for the interface was that it would behave like a glass fiber when near the fiber and similar to the resin when in contact with the resin. CZM was employed here as well when considering the bond between the interface, fiber & matrix.

Table 4: Input properties for three phase model where interface is modeled as a separate entity

Material	Modulus (GPa)	Tensile Strength (MPa)	Poisson's ratio
E-CR-glass	81	-	0.2
Epoxy Matrix	4.2	-	0.3
Interface(Fiber Dominated)	4.2	-	-
Interface (Fiber/resin Average)	42.6	-	0.3
Interface(Resin Dominated)	4.2	-	0.3
Fiber-Interface (Cohesive Zone)	50	40	-
Matrix-Interface (Cohesive Zone)	3.5	10	-

A pressure load was applied on the free end of the fiber and shear stress distribution across the fiber, interface and the matrix was recorded. The boundary condition was applied to mimic a fiber pull out where the bottom part of the matrix block is fixed and the fiber is pulled from the top end. Symmetry about the axis is also considered since it is axi-symmetric model. Since higher strengths was provided in the fiber-interface zone (Modulus 50 GPa) it was observed during the analysis that debond does not take place in this zone but the debond takes place in the interface-matrix region(3.5 GPa). Figure 9 shows the shear stress distribution across the model. This was

based on the assumption that interface takes the property of the fiber in this and the interface fails mostly in the matrix region, if the interface itself is not the weakest link.

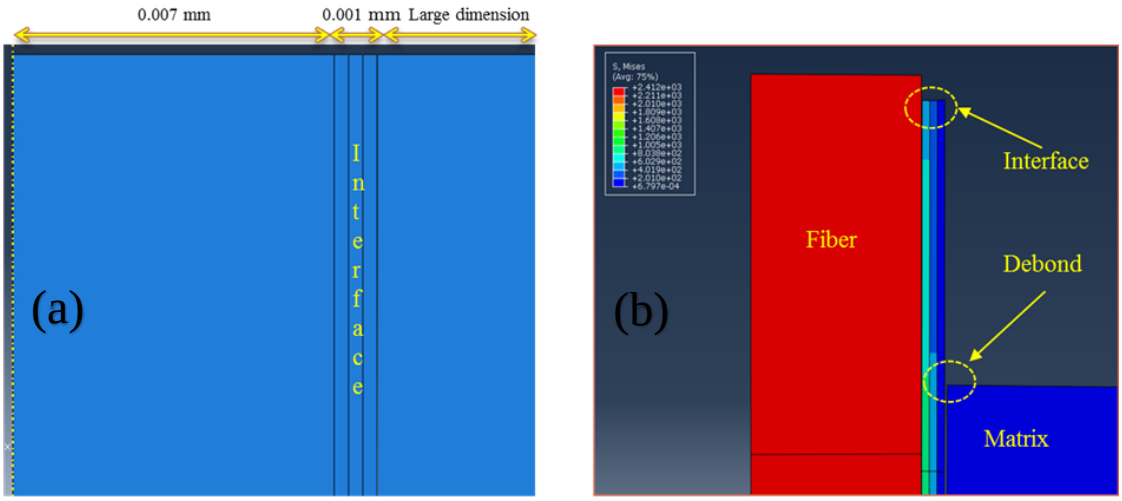

Figure 11 (a) represents the dimension of the unit cell model, Fig 11 (b) represents the debond stage in the simulation process. The stress contour plot is also seen here

The 2D axi-symmetric model covers the entire range of intricacies involved in adhesion of the fiber and the interface and the matrix. It was observed that the interface- which was modelled as a thin film between the fiber and the matrix continued to remain bonded with the fiber. Fig 12 shows a stress contour plot of all three section of the model, as discussed above the stress is mostly borne by the fiber and then then it gradually comes down. The stresses calculated were 1980 MPa, 1870 MPa, 785 MPa, 39 MPa & 11MPa for fiber, fiber dominated interface, average interface, resin dominated interface and the matrix respectively.

The CONTACT STATUS (CSTATUS) feature of ABAQUS was used throughout the analysis between the bonded surfaces. It is divided in three parts- ‘stick, slip & open’. The CSTATUS provides an indication (a) when the contact is closed and is intact; (b)

when it has begun degrading; and (c) when it is completely open. Figure 11 illustrates the contact status at various stages of the analysis. At the initial stage, the contact is entirely intact between both the surfaces; in the middle stage of the analysis, progressive debonding takes place between the interface-matrix zones.

With the application of CZM this model very well demonstrated a single fiber pull out process. Availability of more data sets from exhaustive tests would make the model more robust and it could be used for further investigation of adhesion between the fiber, interface and the matrix.

Even though the finite element models developed herein were for glass fibers, the same methodology can also be employed for carbon fibers. The parameters that would change are- radius of the fiber, dimension of the matrix block, friction coefficient and interfacial crack initiation shear stress. More details on modelling parameters can be found in ref [66]. In this work the authors have followed cohesive zone modelling approach and simulated a single carbon fiber pull out using commercial finite element package Abaqus.

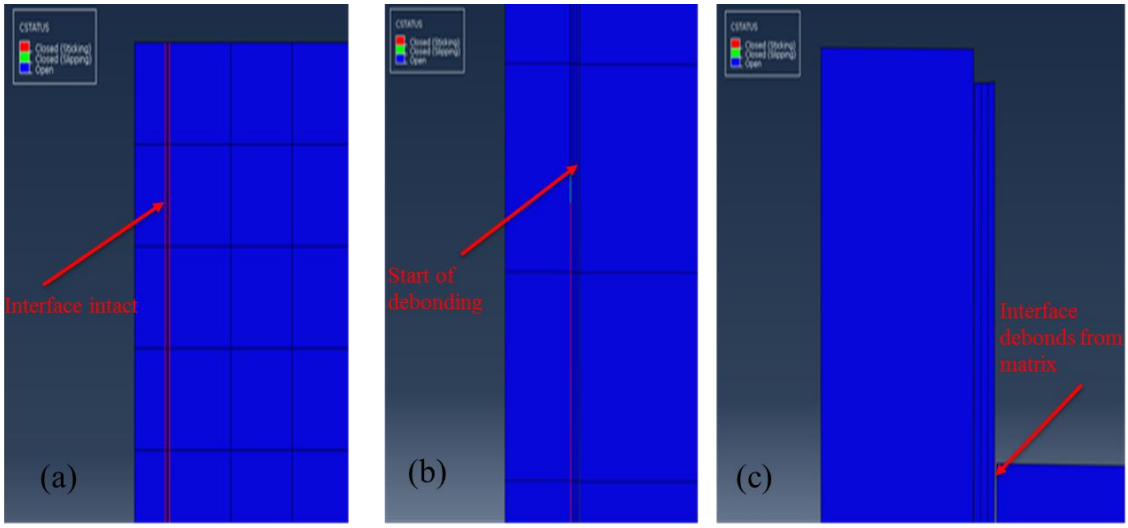

Figure 12: (a) Represents in the initial stage of pull out where the red part indicates the interface intact, Figure 12 (b) represents the middle stage of simulation where absence of red spots indicate debond and Figure 12 (c) represents the debond between the matrix and interface

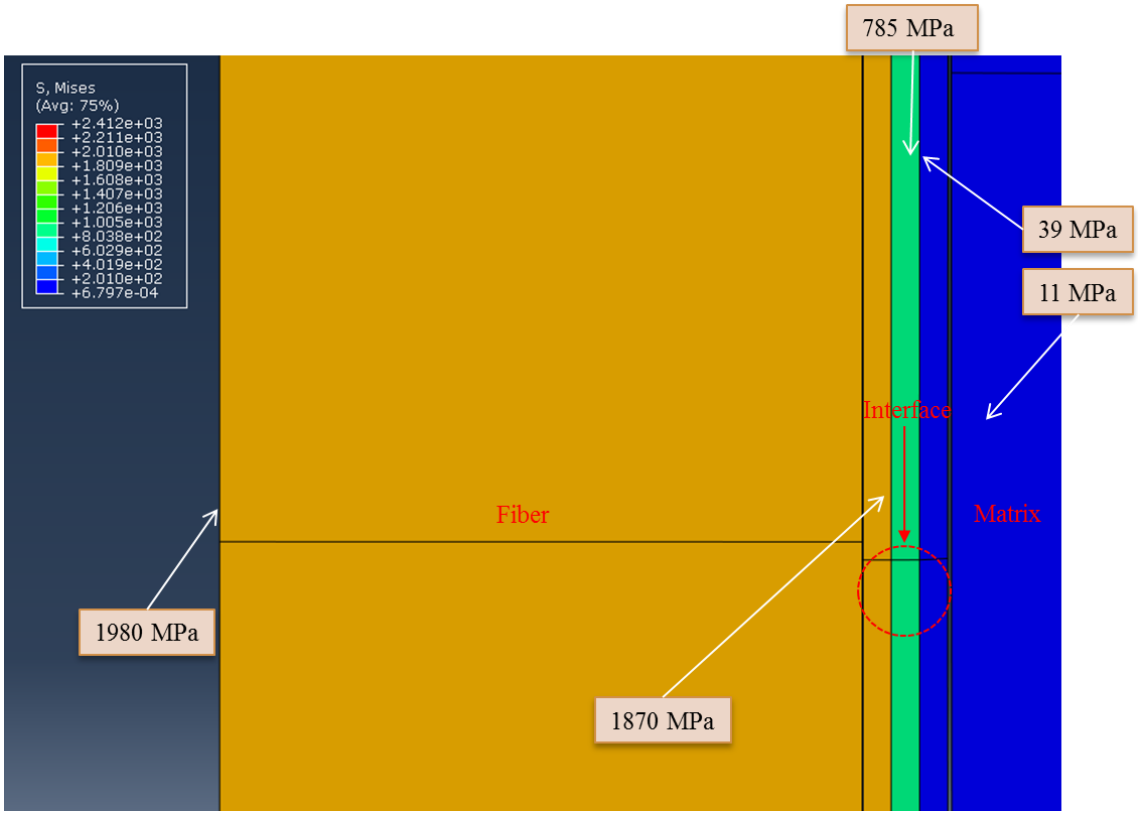

Figure 13: Stress values calculated during the simulation for each sections (fiber, interface and the matrix)

4. OBJECTIVE II: SURFACE CHARACTERIZATION OF CARBON FIBERS

4.1 Introduction

The use of AFM on Carbon Fiber Reinforced Plastics (CFRP) composites to study the interphase is rarely seen in literature. However, there are few research articles, which characterize the fiber/matrix interphase where the focus is on, glass fibers sizing [67, 68]. Tapping mode AFM and nanoindentation was used by Gao & Mader [67] to study sized fiber surface topography and difference in mechanical property in the interphase of E-glass fiber reinforced epoxy resin matrix and modified polypropylene matrix composites. They observed that the interphase region was markedly different from the glass or the matrix region. Moreover, interphase was not formed with unsized fibers. Mai et al [68] calculated a thickness of about 1μm for the interphase region. Elastic modulus and thickness of the interphase for MPS sized glass fiber/vinyl ester resin was also investigated using nanoindentation tests by Kim et al. [21] Hodzic et al. [20] used nanoindentation on glass/phenolics and glass polyester resins.. Smiley and Delgass used atomic force microscopy to investigate the topographical changes of carbon fibers when exposed to low-temperature, low-power, and oxygen plasma treatments [69]. Through their research, it was found that the grooves present in the AFM images of untreated

fibers were the same as those seen by the SEM. The axial grooves were unevenly spaced from 40 nm to 120 nm apart and had a distribution of depth from 1 nm to 7 nm.

All these techniques utilizing AFM, however have been used on fiber-matrix laminated samples, except Dey et al. [7] This recent article explored the use of AFM on single glass fiber filaments with sizing and without sizing. The researchers recorded changes in fiber surface morphology and compared the effect of silane coupling agents and film former on the properties of glass fiber/epoxy interphase.

To study the effect of fiber surface finish on different types of carbon fibers and anticipate their adhesive interaction with the matrix, different characterization techniques were used. AFM was used to measure fiber surface roughness, Young's modulus of the organic coating (sizing) was also measured using Force distance spectroscopy. This enabled in calculating Young's Modulus using the Hertz model [14, 16] and also hardness of the fiber surface using Oliver & Pharr model [69]. Scanning electron microscopy (SEM) images for single fibers was also undertaken to validate the surface morphology and measurement of the diameter. Furthermore, wettability analysis and FT-IR spectroscopy analysis was also conducted to study the fiber wetting mechanism with Vinyl ester resin and difference in elemental composition, if any between different types of carbon fiber respectively.

4.2 Materials & Methods

Six different types of Carbon fibers having different precursors, different mechanical properties were obtained from Oak Ridge National Lab (ORNL). All these fibers were manufactured at ORNL's Carbon Fiber Technology Facility (CFTF). Another commercially available carbon fiber from Mitsubishi Rayon was also analyzed under AFM to compare the results with ORNL fibers. The average diameter of fibers is believed be to be around 7μm based on topographic images. Further investigation was carried out using SEM to measure individual fibers. Fig. 21 provides more details on the diameter and surface of these fibers. The diameter for Mitsubishi fiber was found to be 7 μm from a research article by Dong et al. [70] . Table 4 provides details regarding the fiber used for this work. The first three samples are similar in the type of precursor used but the tow size is different. All the sample were pre-chopped to a size of 38 mm except, sample B12, K30-HTC, and K-15U Plaited. The size and form of the fiber are believed to not make any impact since the AFM characterization is done on a very small scale (5μm)

An AFM (XE-70) was used as both a fiber surface imaging tool and a nanoindentation device. The topography of the samples was studied in tapping mode at a resonant frequency of around 60 Hz, using a silicon cantilever (ANSCM-PT) coated with platinum. This probe is used specifically for force modulation. The nominal spring constant of the cantilever was 3 N/m, a tip radius of curvature (ROC) 30nm and the shape being pyramidal. Samples were prepared by separating single filament of fibers from the tow and sticking on to double sided tape.

The 3D view is unique to Scanning Probe Microscopy (SPM) is different from other microscopic techniques such as SEM or TEM. . The SPM scans the sample surface

horizontally (x, y) line by line while collecting the vertical (z) direction profile of the sample surface. As a result, the SPM collects truly 3-dimensional (x, y, and z) information from the surface and this 3-dimensional data represents true surface topography [14].

Table 5: Types of Carbon fibers analyzed under the AFM

Carbon Fiber Type	**Tow Size**	**Form**
B48	48K	Chopped
B24	24K	Chopped
B12	12K	Continuous
K30-HTC	30K	Continuous
K-12U	12K	Chopped
K-15U Plaited	15K	Continuous
Pyrofil (Mitsubishi Rayon)	12K	Continuous

Ten images were taken for each samples and average roughness and root mean square (RMS) roughness values were calculated at various spots using XEI 1.8 (Image processing software from Park Systems). For each image, five roughness readings were taken horizontally along the fiber surface which was averaged to obtain the final values. Roughness parameters derived from ASME B46.1 (American Society of Mechanical Engineers, surface roughness, waviness and lay) were calculated based on the following definitions. Image mean roughness (R_a) is the arithmetic average of the absolute values of the surface height deviations, measured from the mean plane. Equation 5 and 6 describe the method of calculation of average roughness and root mean square roughness respectively [71]. AFM images with a scanning size of 5μm was recorded for topography, phase and nanoindentation purposes.

$$R_a = \frac{\sum_i^n |z_n|}{n} \quad (5)$$

$$R_q = \sqrt{\frac{\sum_i^n (z_n)^2}{n}} \quad (6)$$

In equations (5) and (6), Z_i values represent all the "n" deviations in surface height measured from the mean data plane in the AFM image [14]. It should be noted that two surfaces with different frequency of peaks can have the same average R_a and/or R_q values [72]. Nonetheless, surface roughness values provide quantitative information that complements the information provided by phase image depth analysis alone.

The mechanical properties of the sizing on the fiber was determined using nanoindentation or force distance spectroscopy mode of AFM, which measures the load F and penetration depth *h.* The AFM imaging tip was forced perpendicularly on to the fiber surface at a frequency of 60 Hz and to a selected maximum force ranging from 50nN-77nN. Analysis of force-distance spectroscopy during approach and retraction provides us with quantitative measurement of different interaction forces acting between the tip and sample [16].

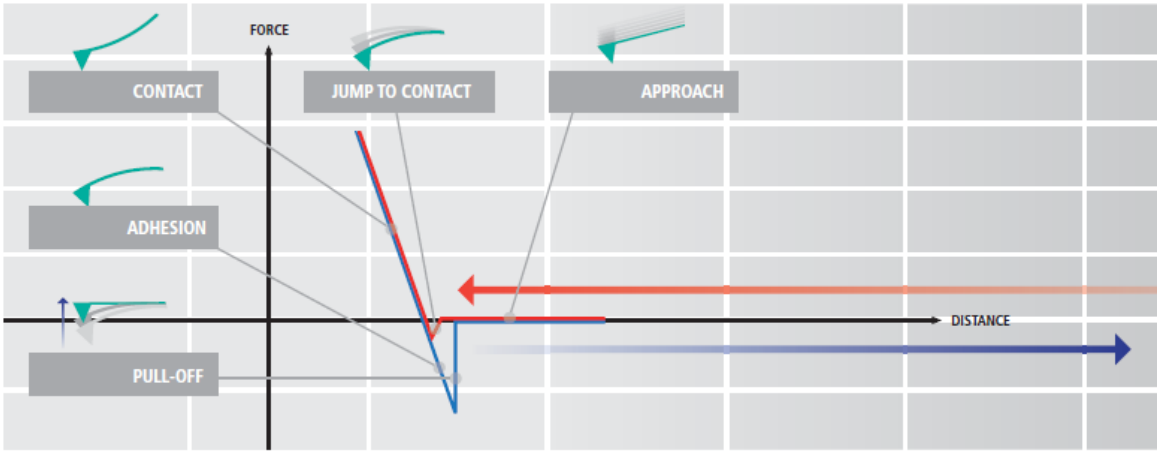

Figure 14: Schematic of a typical force-distance curve obtained using AFM [69]

Hertz model was used to calculate the Young's modulus for the sizing coated on the fiber. XEI 1.8 has an in-built FD spectroscopy mode where the mechanical properties can be calculated after providing the inputs as given in Table 2. For a non-adhesive elastic contact between a stiff sphere of radius R (in this case the tip) and an elastic half-space (Young's modulus E, Poisson's ratio ν), the Hertz-model predicts the force as a function of the indentation δ. Hertz model is represented as follows,

$$F = \frac{4E}{3(1-\nu^2)}\sqrt{R\delta^{1.5}}. \quad (7)$$

Oliver & Pharr model[69] which is the common model used to calculate hardness for nanoindentation was used here. The area of the residual indentation in the sample is measured and the hardness, H, is defined as the maximum load, $P_{max,}$ divided by the residual indentation area, A_r which is given as under,

$$H = \frac{P_{max}}{A_r} \quad (8)$$

Table 6: Input parameters used in Hertz & Oliver-Pharr model for calculation of mechanical properties

Input Parameters	Value
Poisson's ratio of the sample	0.30
Poisson's ratio of the tip	0.07
Tip Shape (Hertz Model)	Parabolic
Radius of curvature for the tip	10 nm
Tip Shape (Oliver &Pharr Model)	Berkovich

4.3 Surface Topography

A surface contour plot of single carbon fibers, 5μm by 5 μm, along the vertical section (along the length of the fiber) for all our samples are shown in Figures 14. Ridges or striations can be seen down the length of the fiber on all the six samples. Striations are a common phenomenon on Carbon fiber surface and have been observed by various researchers studying the topography of carbon fiber surfaces [5, 12, 32, 71, 73]. The sizes of the ridges varied slightly and the edge contours did not appear to be consistent. It was also seen that these striations were more prominent on the first three carbon fiber samples when compared to the last three. The first three samples shared the same Bluestar carbon precursor. The "K" fibers have different precursor which is Kaltex. All topography images taken by AFM were 2^{nd} order plain fitted to account for fiber curvature. A similar approach to account for fiber curvature while processing AFM images was taken by Dey et al [7] in their study on glass fiber surfaces. This was done using XEI 1.8 image processing software. While looking at the flattened topography image plots (Figures 15) it was noted that the ridges were present there as well and it was not a function of the

fiber curvature. The striations on these fibers tend to be covered by bumps on the fiber surface as well (Figure 14) furthermore it was worth noting that these bumps were present more or less on all of our samples. The bumps did not appear to have a regular pattern. Also, individual bumps on the fiber surface were seen in greater concentration on K fibers. It was also observed by Leon et al [71] at Hexcel corporation in their recent patent that the striations on the carbon fiber surface is also related to their mechanical property. It was noted by the authors that these striations lead to better tensile modulus and strength. On the other hand it was observed by N. Dilsiz and J.P Wightman [5] that these striations decreased with applications of PTPO & Ultem® sizings on the carbon fiber surface which in turn led to better surface roughness and hence better interfacial properties for the final composites.

When comparing the AFM images to the more common Scanning Electron Microscopy (SEM) images (Figure 17), it was noticed that the same ridges and raised defects on the fiber surface were present in all the carbon fibers (although image reproductions may make SEM feature identification difficult). It was evident, however, that the AFM images do permit a much closer look of the fiber and allow for quantitative height measurements to be made on each peculiarity .

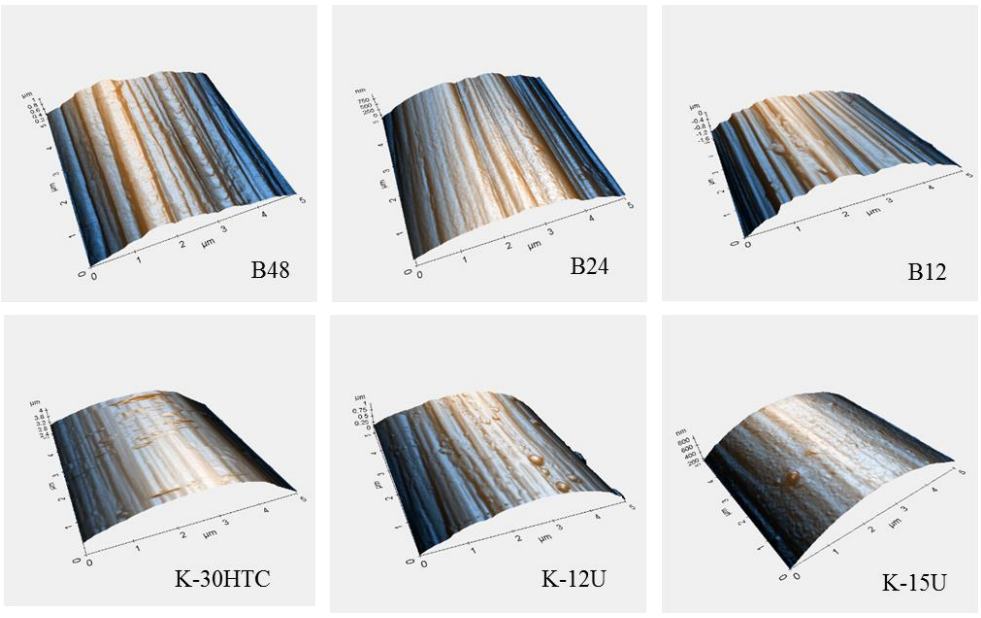

Figure 15: 3D enhanced topographic images. The lighter color represents higher height of the fiber surface while the brighter color (blue in this case) represents lower height of the fiber surface

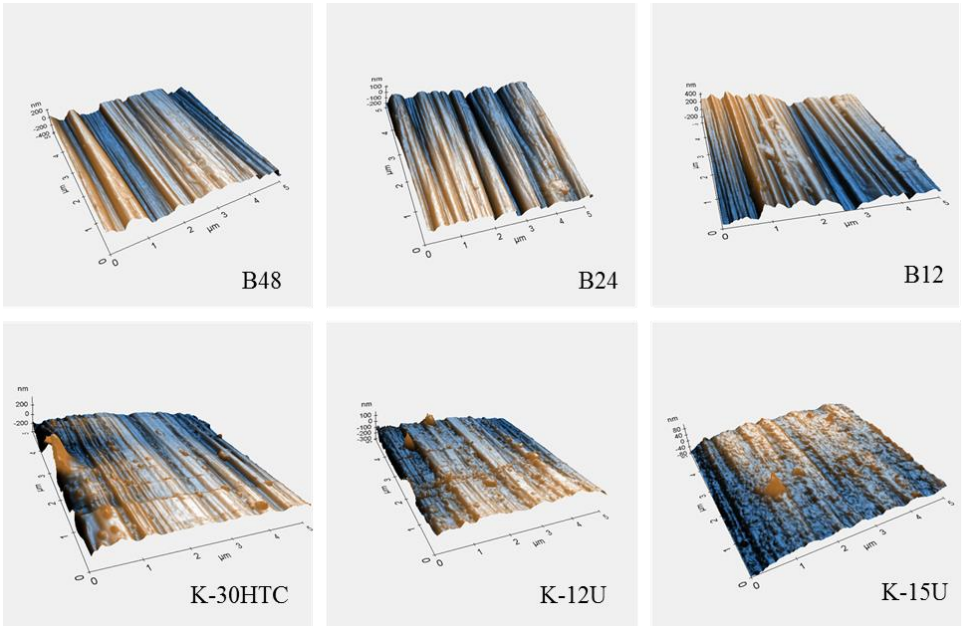

Figure 16: Second order plain fitted topography images of various carbon fiber samples The lighter color represents higher height of the fiber surface while the brighter color (blue in this case) represents lower height of the fiber surface

Phase contrast microscopy, using AFM, was used to detect and quantify changes in composition across the polymer layer deposited on the fiber surface. The technique takes advantage of the contrast in viscoelastic (viscous energy dissipation) properties of the different materials across the surface [74]. Phase patterns are also be used to differentiate between regions of strong and weak surface-tip interactions. These regions may in turn be related to material features such as, e.g., crystalline domains [71]. When combined with topography, it becomes a powerful tool to understand the surface behavior of the samples. For all our samples, phase image and topography were in good correlation with each other. The default palette used in our analysis using XEI 1.8 image processing software is based on gold color palette scale in which darker colors indicate lower heights and the brighter colors indicate higher height values. The 3D images along with enhanced view in color palette provide a realistic view of the coating on the fiber surface.

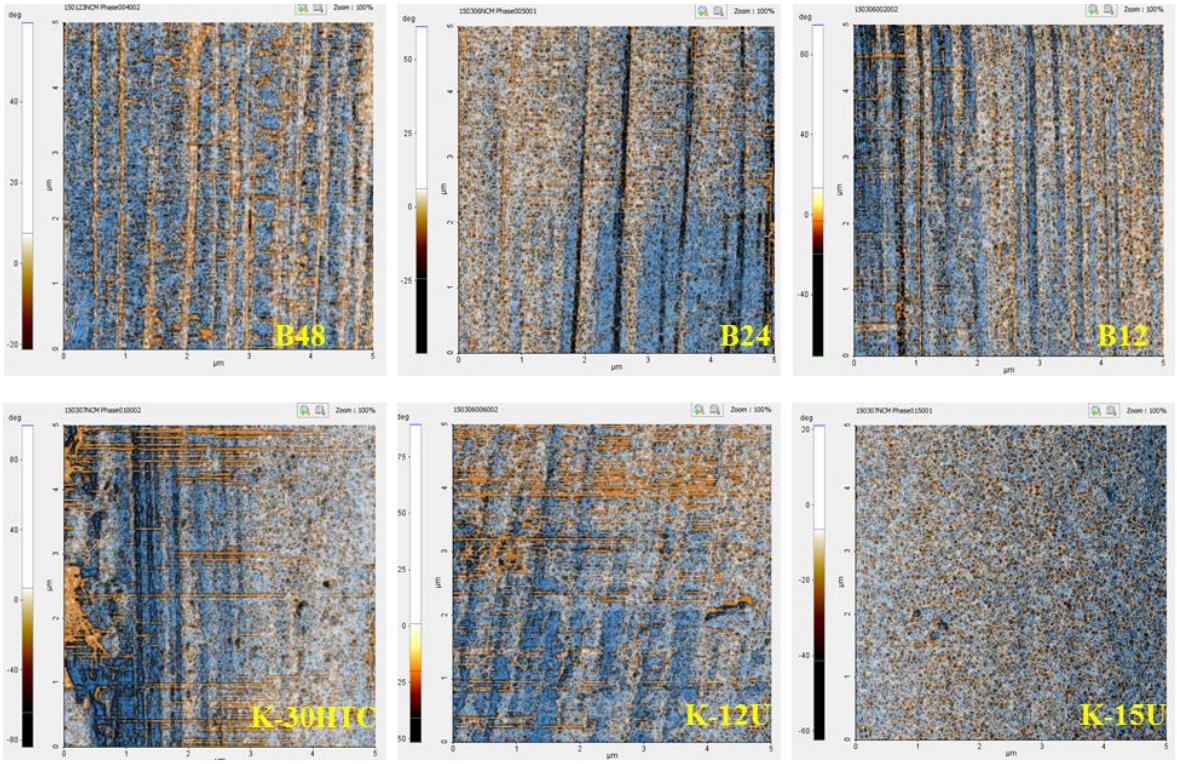

Figure 17: Enhanced phase image; Different color represent change in height of the sizing deposited. Lighter color represents higher height and brighter color (blue) represents lower height

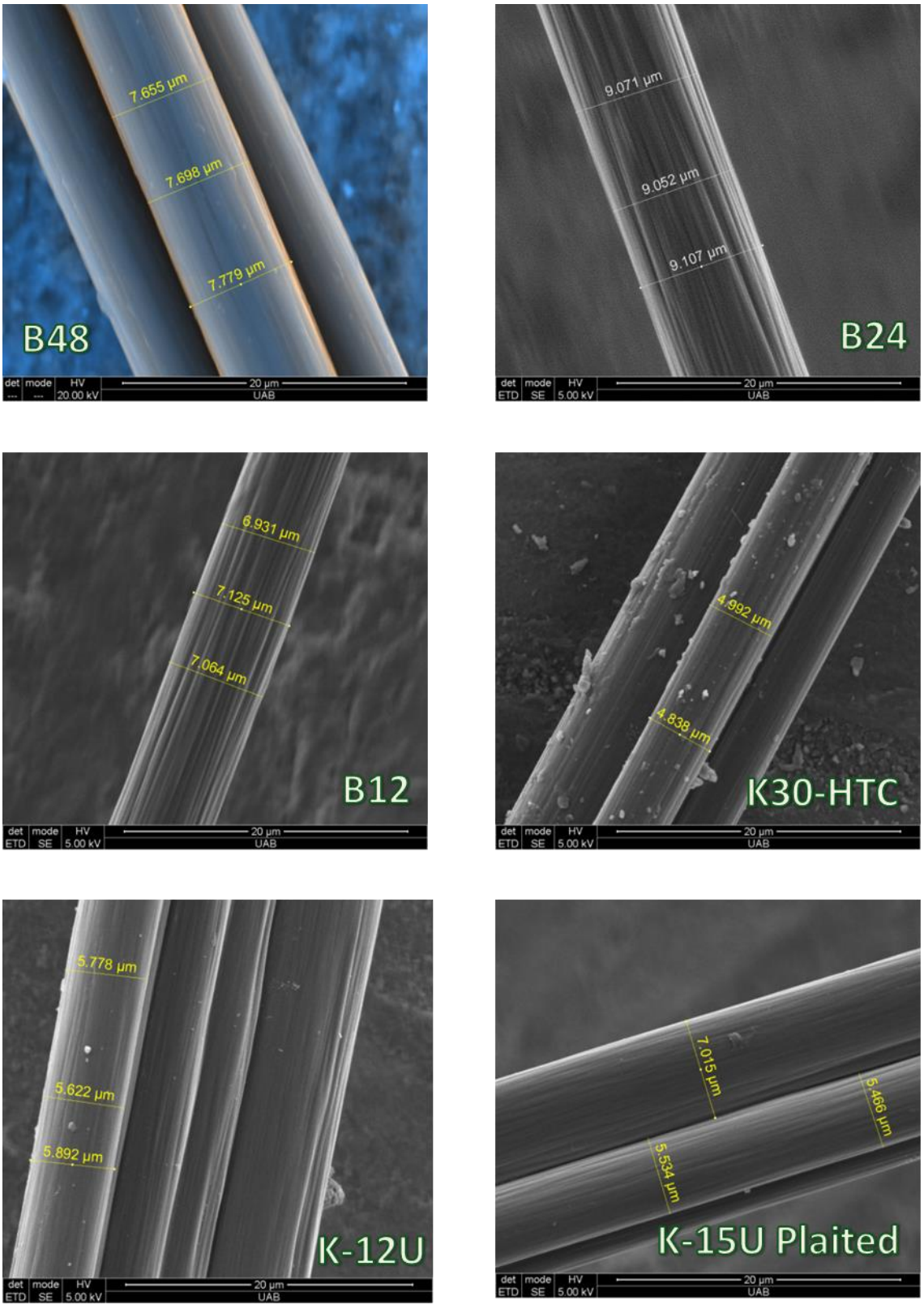

Figure 18: SEM images for different carbon fiber types used for surface characterization

To compare our topography images obtained from AFM, a commercially carbon fiber manufactured by Mitsubishi Rayon (Pyrofil TR 50S12L) was also scanned under AFM. Fig. 18 below shows the topography and phase images for this fiber. In terms of surface characteristics, there was no striking difference. The striations on the surface were less evident but that did not make any difference in roughness and mechanical properties which are discussed in the next sections.

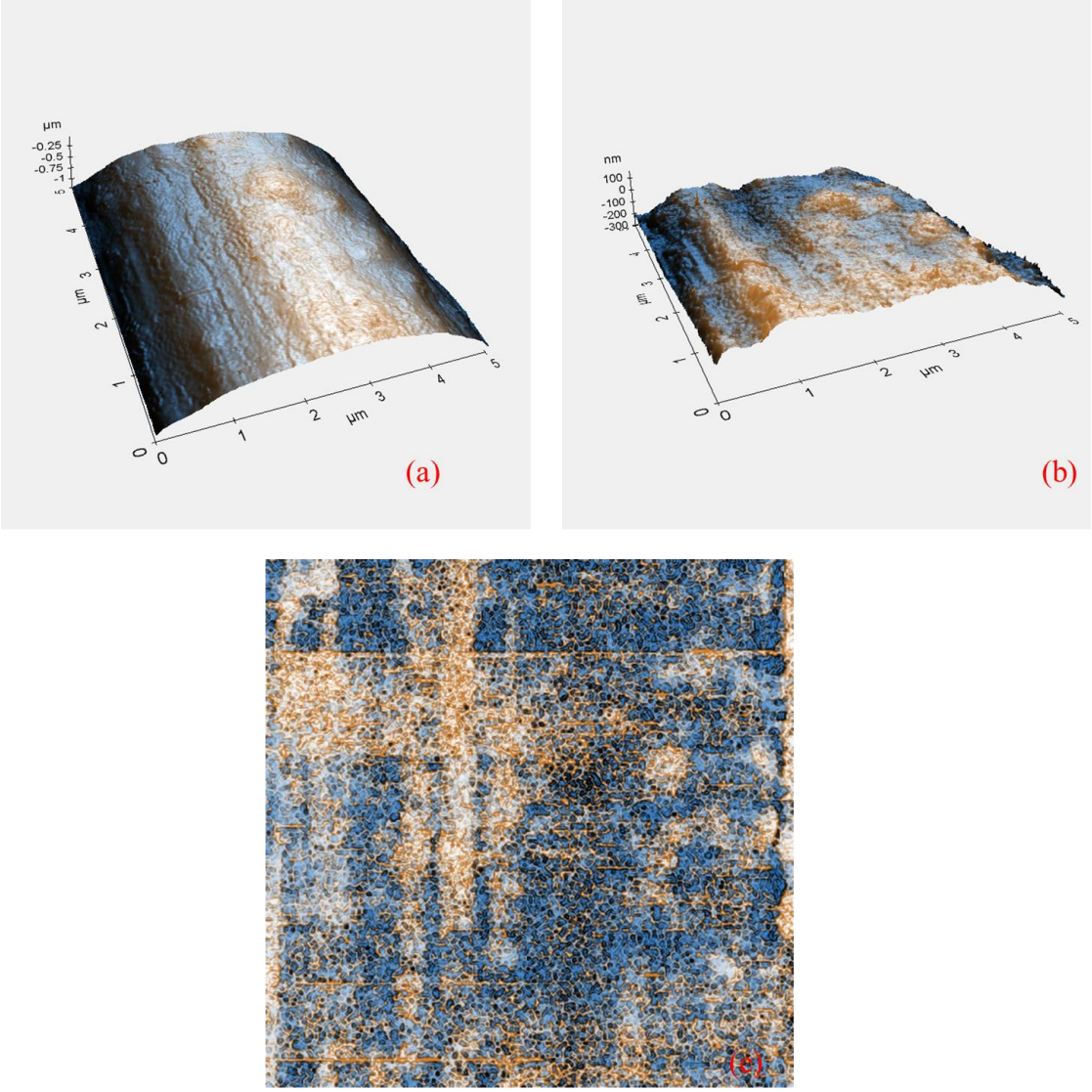

Figure 19: (a) Topography of Mitsubishi Rayon Carbon fiber, (b) Flattened topographic image fit to second degree, (c) Phase image of Mitsubishi Rayon carbon fiber

4.4 Surface roughness of Carbon fibers

To characterize fiber surface features with sizing on it, surface roughness was examined. The roughness values (average & RMS) calculated for all the six samples along commercially available Mitsubishi carbon fiber are shown in Figure 17 below.

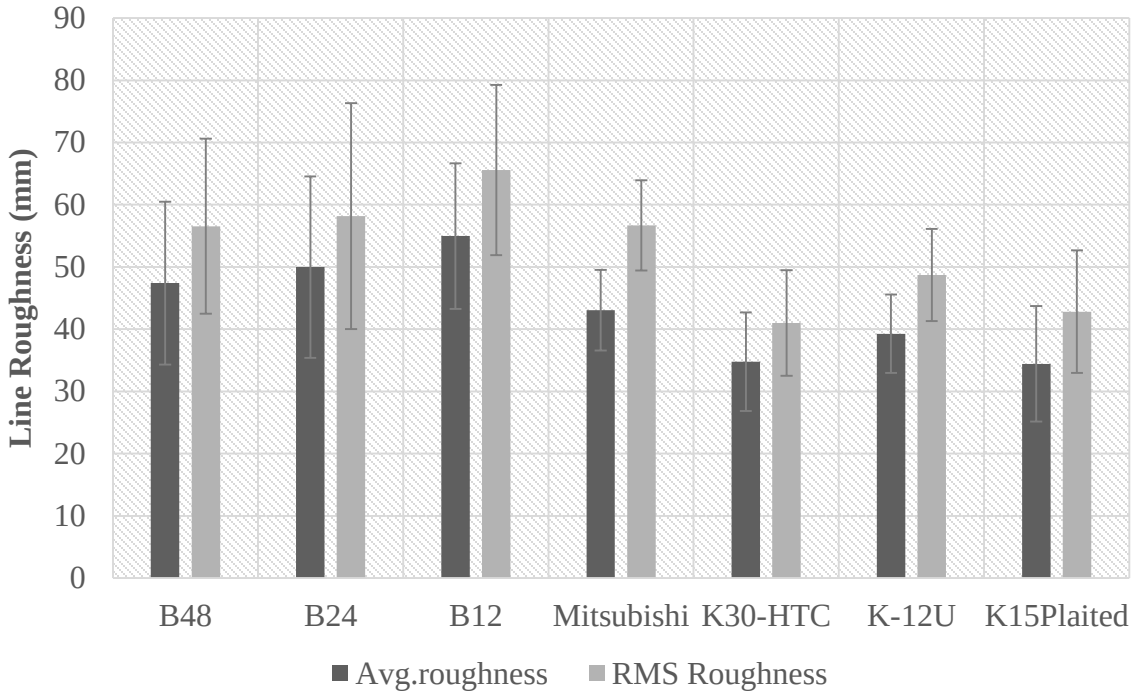

Figure 20: Average roughness and RMS roughness for different carbon fiber samples

As discussed in the previous section about two different precursor systems used in manufacture of carbon fiber sample, the roughness values were also on the same line. The "B" fibers had the highest mean surface roughness values (R_a). B48 had an average roughness of 47.41 nm, while roughness calculated for B24 and B12 were 49.98 and 54.97 nm respectively. This was expected since the precursor being same and also the sizing was same for these fibers, which was investigated using FT-IR. The results for FT-IR are discussed in section 4.6. For all the six carbon fiber samples from ORNL, the

roughness values were calculated on flattened images. Different roughness values were attributed to longitudinal streaks or striations. As discussed in the previous section, the striations were more prominent on "B" fibers, hence it was concluded that these fibers had higher roughness. Commercially available Mitsubishi Rayon fiber was also analyzed under the AFM to compare our results and the roughness value was calculated to be 43.05 nm. The "K" fibers were very smooth with roughness values in the range of 30nms. Even when visually inspected these fibers showed a very smooth surface.

Previous research by Dey et al [7] show that surface roughness is an important factor in determining strength & energy absorption of the interphase. Y. Luo et al. [73] in their study of CCF 300 carbon fibers found the roughness values to be 88.493 nm,71.698 and 58.877 for different samples. The scan width was 3µm x µm for their test. Comparison of our results with the findings of Dilsiz & Wighman [5], it was found that our roughness values were high (30-55nm). They reported a mean roughness of 9 & 15 nm for Ultem® & PTPO® sized carbon fibers while, the roughness values for unsized fibers was 7.5 nm. The images were scanned with the dimension being 1µm x 1µm. This could be a potential reason for our roughness values not being similar. Gao et al [12] also reported a mean roughness in the range of 4nm, although the scan was not done on single fibers but on carbon epoxy composites. Gao et al [12] also stated that the surface roughness in a few tens of nanometer scale has no remarkable contribution to interphase adhesion from the mechanical interlocking. There is a need to delve deeper to understand the reason behind these different roughness values.

Gao et al [12] previously reported that PAN based IM fibers with small graphite planes have much higher surface area difference ratio than HM fibers. A similar

observation was observed for AS4 carbon fibers[75]. It was reported that AS4 fibers have homogeneous surface. The chemistry of fiber surface is greatly influenced by presence of hetero atoms (hydrogen, oxygen, nitrogen, halogens, sulfur, phosphorus, etc.) situated at the edges of the graphite layers[12]. The polarity of these groups is mostly influenced by neighboring chemical structure, in turn resulting in acid/base character of the carbon surface. This explains the higher surface roughness for some type of carbon fibers [37]. Previous research on glass fiber sizing gives us an insight into ways of increasing the surface roughness by including γ-APS sizing with polyurethane film former as reported by Mai et al. [68].

4.5 Mechanical Characterization of the fiber surface using Force-distance (FD) spectroscopy

Force-distance (FD) spectroscopy using an AFM is a beneficial tool to characterize mechanical properties of various materials. A typical FD spectroscopy image is shown in Fig. 20. In FD spectroscopy, the cantilever tip touches the sample surface with a user prescribed amount of force accurately applied using the AFM's Z scanner. The deflection of the cantilever can be used as input to a feedback circuit that moves the scanner up and down in the z direction, responding to the topography by keeping the cantilever deflection constant. An image is generated from the scanner's motion. With the cantilever deflection held constant, the total force applied to the sample is constant. This mode is generally preferred for most applications. The interaction forces can be determined using the force-distance curve obtained by detecting the cantilever deflection when the tip of the force microscope is moved towards and away from the surface. A

force resolution in the range of pico Newton to micro Newton can be achieved in these experiments. In the low force regime, the interactions observed can range from Van der Walls forces in the Nano Newton scale to entropic forces of several hundred Pico Newton. In most of the cases, the interactions occurring are strongly depend on the experimental conditions, such as the tip and sample material, chemical modification of the surfaces, and the surrounding medium.

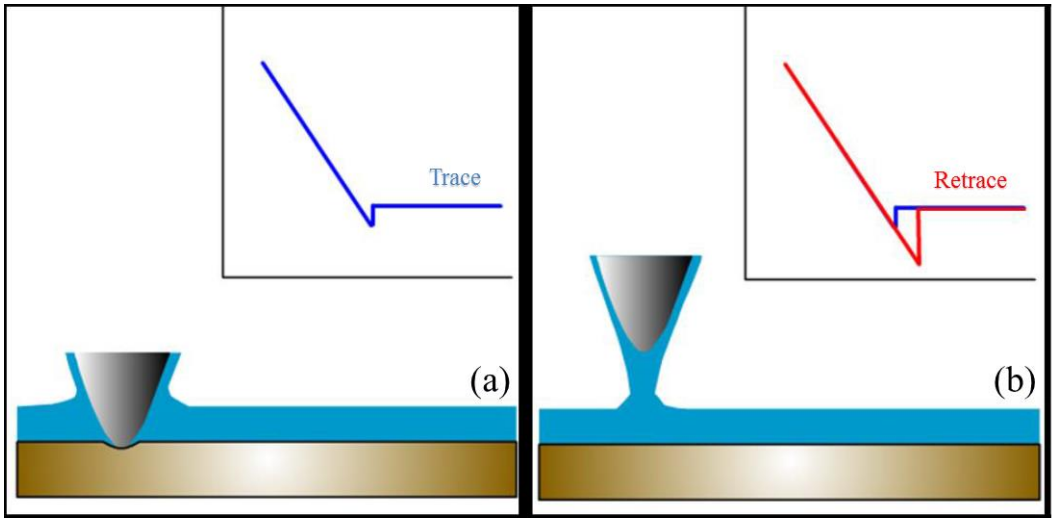

Figure 21: Schematic of force-distance spectroscopy technique. (a) The blue curve represents the cantilever deflection-distance curve obtained while the AFM tip approaches the sample. (b) The red curve represents the cantilever deflection-distance curve. Image adapted from [15]

The application of AFM or any other test method to characterize the mechanical behavior of just the top surface is rarely seen. FD spectroscopy was employed to calculate mechanical properties of the polymer coating (sizing) on carbon fibers. The scan length & width was kept constant at 5µm for FD spectroscopy. Each of the samples were indented at sixteen different spots and Young's modulus, indentation depth &

hardness was calculated using Hertz model and Oliver & Pharr model [69] respectively. This model is in-built in the image processing software XEI 1.8. The results are shown in Fig. 19-21 below. As discussed earlier, a total of thirty two data points were accumulated on the fiber surface to calculate average Young's modulus. Not all the indentations were successful and of all the thirty two points. The assumption here was that since both the fibers are very similar, same composition of sizing must have been used, hence the result. The platinum coated tip used for mechanical characterization couldn't penetrate the hard carbon substrate (images did not show any indentation on the carbon surface), the z axis movement of piezo stage (linear solid curve, shown in color red in fig 18) represents only cantilever deflection and no indentation while collecting force curves.

Samples B48 and B24 showed near identical Young's modulus while B12 showed outlier behavior as seen in roughness results. The Young's modulus calculated for this sample was 2 MPa. This could be due to prominent striations seen on the surface which made it difficult to penetrate hence lower indentation depth and better hardness properties as well. The "K" fibers which are different form the first three Bluestar fibers showed almost similar mechanical properties with Young's modulus values hovering around the 1.20 MPa mark. Comparison with commercially available Mitsubishi Rayon Carbon fiber was also conducted. The Young's modulus was 1.4 MPa and indentation 609 nm.

Analysis of FD spectroscopy during trace and retrace provides a quantitative measurement on the different kinds of interaction forces acting between the tip and the sample [76]. Van der wal forces were observed in FD spectroscopy while tracing in all the samples. Equation (9) below gives the mathematical expression for the forces encountered. Retrace does not normally follow the same trace and hysteresis is

experienced [15]. For our carbon samples in retrace mode, the majority of the forces encountered were adhesion and capillary force. The equations (10 & 11 respectively) are given below. The source of adhesion depends mostly on the nature of the sample and the radius of the probe sphere. A large negative deflection is also experience in case of adhesive forces. The only difference between adhesion forces and capillary forces are greater force and more interaction. More information can be obtained from ref [76]. More force is required for the probe to retrace is step due to larger surface tension between the probe and simple. K30-HTC & Mitsubishi Rayon samples experienced adhesion force while the rest samples experienced capillary forces which is attributed to a formation of water bridge between the tip and sample [76].

$$F(D) = \frac{AR}{12D^2} \tag{9}$$

where, A is Hamaker constant, R is the radius of probe sphere and D is the probe-sample separation distance

$$F = -3\pi R\gamma \tag{10}$$

where, γ is the surface energy between the tip and sample.

$$F = 4\pi R\gamma_L cos\theta \tag{11}$$

where, γ_L is the surface energy of the liquid and θ is the angle related to the geometry of tip-sample contact

Previous research on this subject indicates the interphase thickness to be in the range of 800-1500 nm [21], the indentation depth obtained from AFM are in the range of 478-637 nm which showed the validity of obtained results.

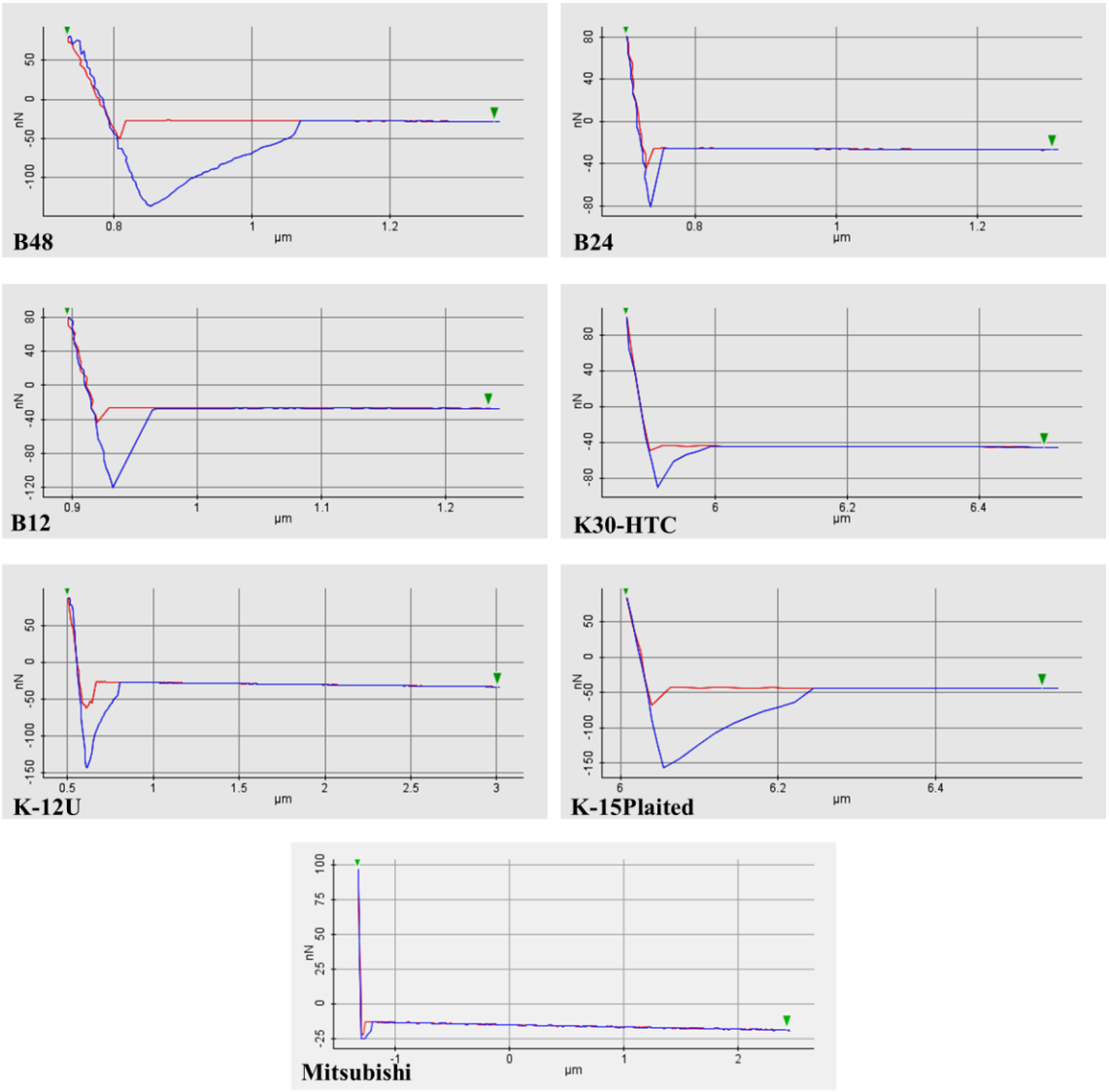

Figure 22: Force distance curve for all seven samples. The red curve represents the trace of the tip o or approach part of the indentation for AFM tip while the blue curve represents the retrace of the AFM probe.

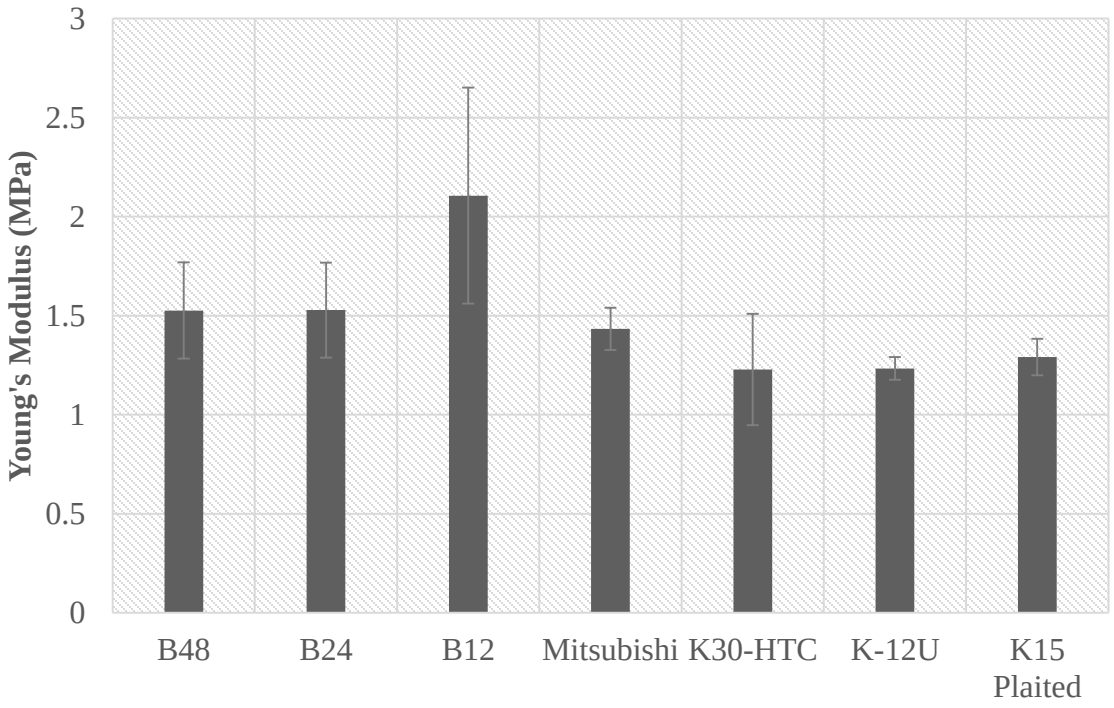

Figure 23: Young's modulus calculated for coating on single carbon fibers

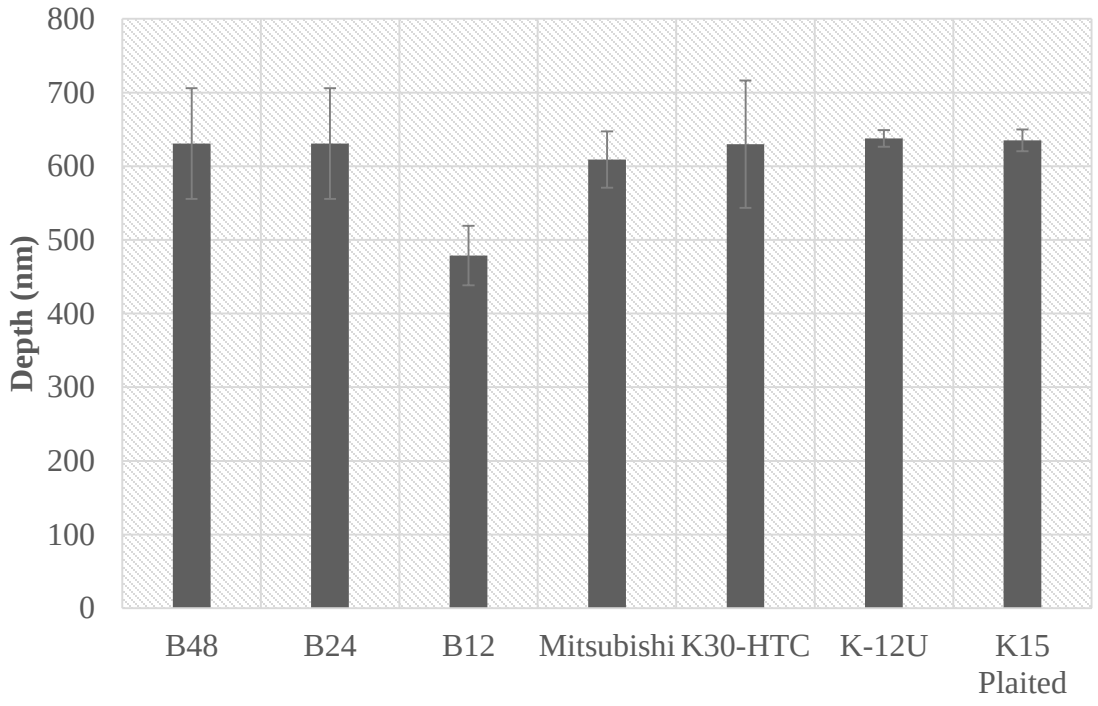

Figure 24: Indentation depth for different carbon fiber samples

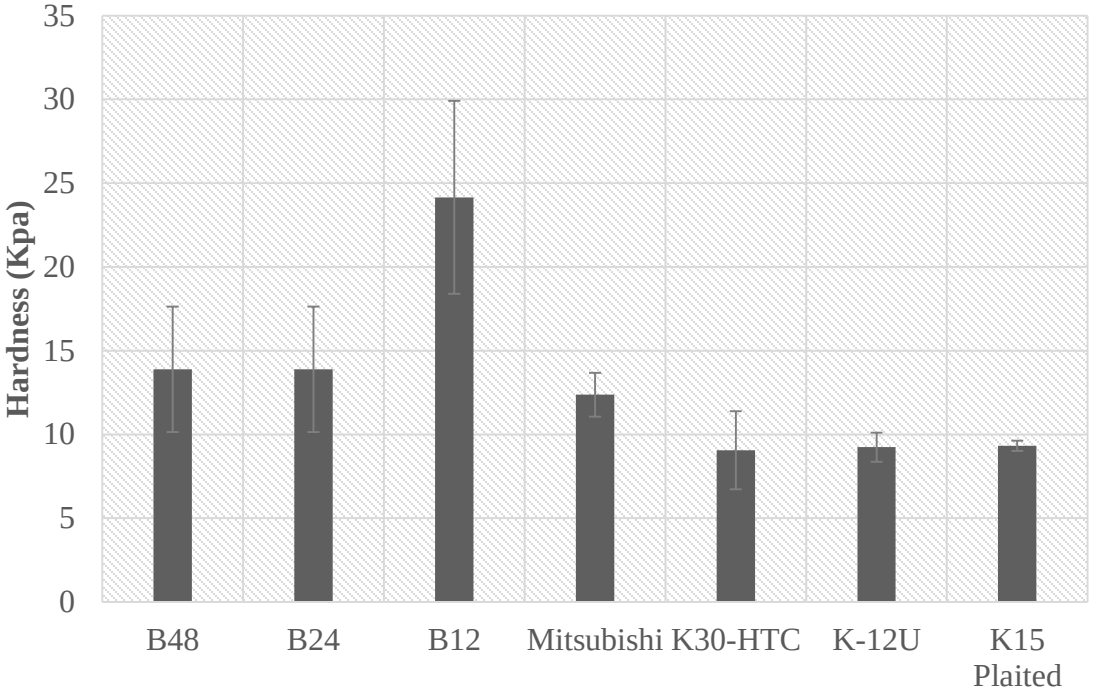

Figure 25: Measured hardness for different carbon fiber samples

4.6 FT-IR spectroscopy on Carbon Fiber surface

The carbon fiber surface is still not well understood due to technical limitation of spectroscopy techniques available. X-ray photoelectron spectrometer (XPS) is a great tool to study elemental composition however it is very difficult to detect minor chemical structure differences which are essential to study the adhesion of carbon fiber surface to the resin matrix [77]. Fourier transform infrared (FT-IR) spectroscopy is also a handy tool and has been successfully implemented to characterize glass fiber composite interface by Ikuta et al. [19] and by Chatzi et al [78] on Kevlar. However, severe scattering and high absorptivity of carbon fibers presents its own challenges but newer techniques such as diffuse reflectance (DR) and attenuated total reflection spectroscopy

(ATR) have been getting acceptance as an alternative method for analysis of carbon fiber surface [77].

FT-IR equipped with attenuated total reflectance has been employed on many occasion [79-81] by researchers studying the effect, different chemical functionalities have on carbon fiber surface. Furthermore, high sensitivity and in-depth data analysis capability of FT-IR contribute much to the carbon fiber surface analysis [32].

Tow of carbon fiber samples were inserted between diamond cells and was set on stage of a microscopic FT-IR spectrometer (Figure 25 shows a photograph of the instrument used). As shown in Fig 26 absorption peaks were identified at 1680 cm^{-1} and attributed to carbonyl stretching vibration of the aromatic carboxyl groups. Morita et al [32] from Toray Inc. found a similar peak in their characterization study on carbon fiber surfaces. The absorption peaks in the range of 2900 cm^{-1}, which were the most prominent ones are related to C-H bonds present in CH, CH_2 or CH_3. Further literature review on this subject revealed the possibility of CH_2 stretches were more plausible than C-H vibrations [77]. Wide peaks in the region of 3300 cm^{-1} were attributed to possible O-H bonds. Small shoulders in samples B48, B24 & B12 were identified at 3700 cm^{-1}, this could be due to presence of N-H groups (either 1° or 2° amines) on the surface. Noise in the signal which was seen in the region of 2000-2300 cm^{-1} was due to machine defect and had no relation whatsoever with the samples.

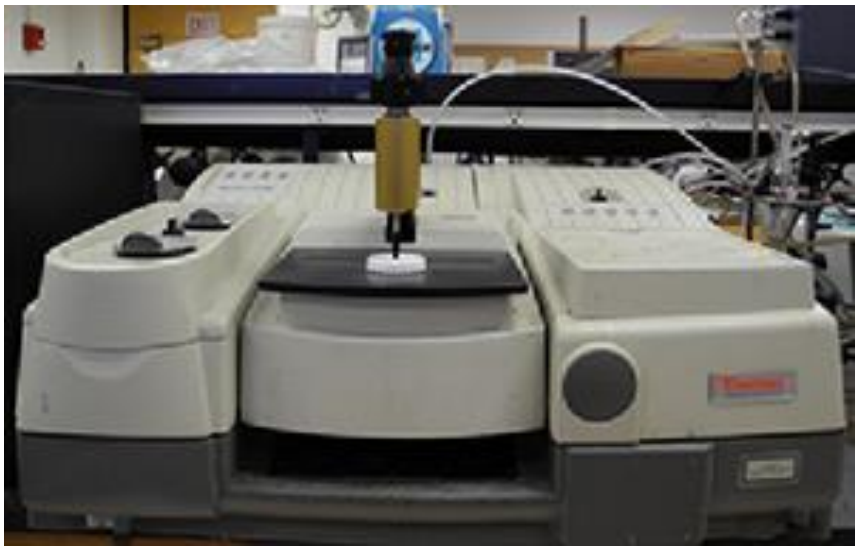

Figure 26: Image of Thermo Scientific Nicolet 4700 FTIR with a Smart Orbit Attenuated Total Reflectance (ATR) accessory

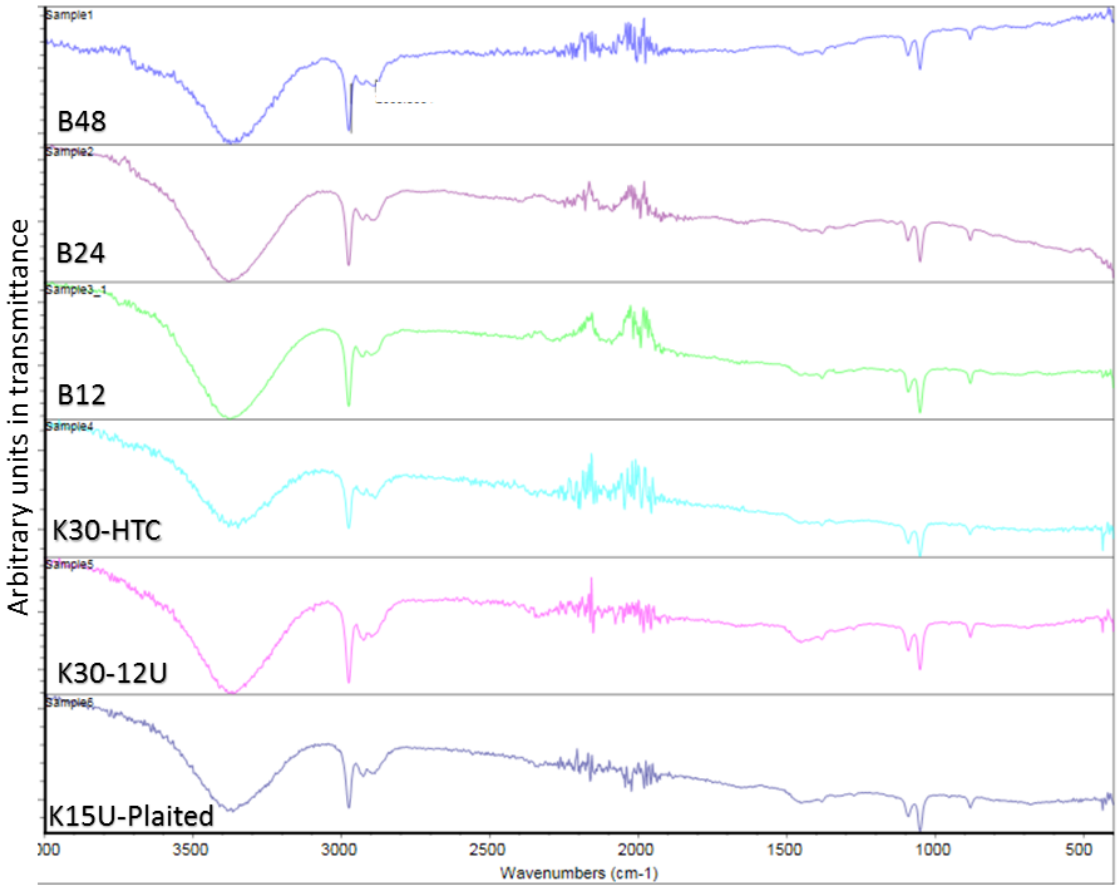

Figure 27: FTIR scans for different carbon fiber samples

4.7 Wettability study on single carbon fiber filaments

The shear strength of carbon composites is greatly influenced by wettability [82]. When the liquid resin wets the fiber adequately a large interfacial area of contact is established which promotes strong bonding between fiber and the matrix. To study the wettability characteristics of a solid surface, contact angle is generally calculated using conventional telescope-goniometer method, the Wilhelmy balance method, and the more recently developed drop-shape analysis methods. Contact angles << 90° generally represent high wettability while angles much greater than 90° represent low wettability [83].

Contact angle was measured using dynamic sessile drop method with a goniometer on carbon fiber surfaces of specimens. The specimens to be tested were placed on a metal platform and the device leveled carefully (Fig 27). The camera was set at 40X (fine resolution) with a white background placed opposite the camera on the leveled stand. The resolution of the camera was adjusted to fine picture quality. After leveling the equipment, a micro pipette was filled with Vinyl ester resin (3µl) and placed 3mm above the surface of the specimen using precise gridlines from the Keyence software. After the camera started recording followed by drop placement, the first angle made by the vinyl ester resin with the specimen surface was measured. The contact angles measured using Keyence software for both samples are shown in Fig. 28 (a) and (b). For sample B24 carbon mats were used and for K30-HTC fiber samples used were in their fiber form. Five readings for contact angles were taken to reach an average consistent value. Average contact angle calculated is shown in Fig 29.

The results for contact angle was used to compare the wettability properties for these two type of Carbon fiber (B and K) and estimate the effect of roughness variation for these two fibers. K30-HTC was observed to have slightly higher contact angle. This was in line with the general belief that lower roughness leads to higher contact angle and poor wettability. Dilsiz and Wightman [5] in their study on Zoltek carbon fibers with different sizings observed that unsized fibers had less roughness and lower contact angles while Ultem® sized fibers had higher roughness and lower contact angles for wettability.

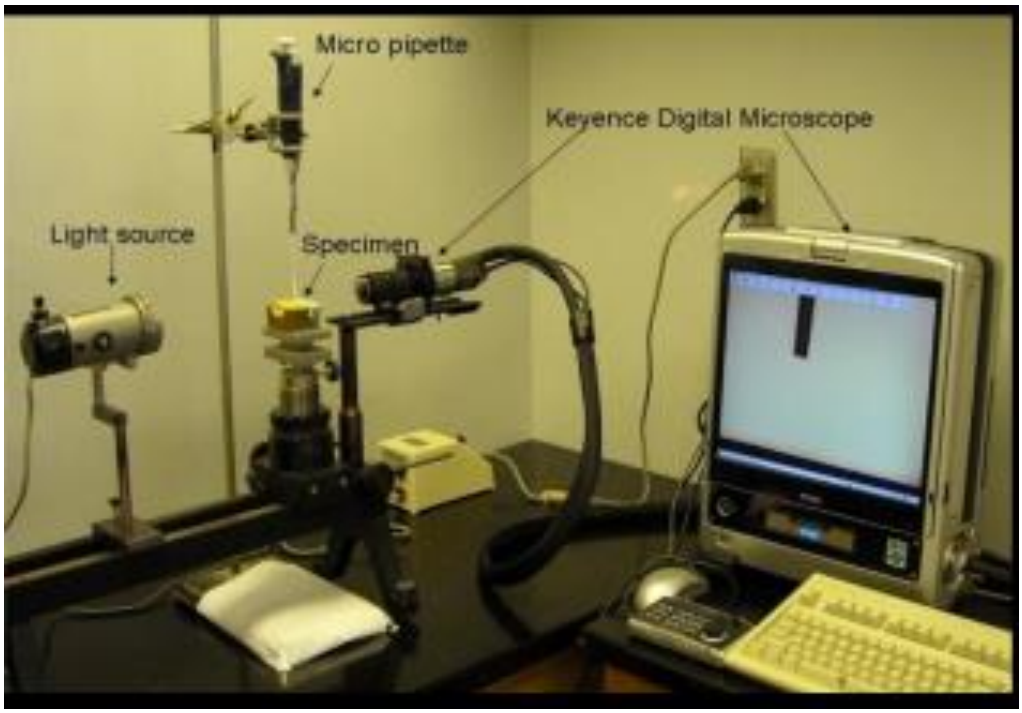

Figure 28: Goniometer setup used to measure contact angle

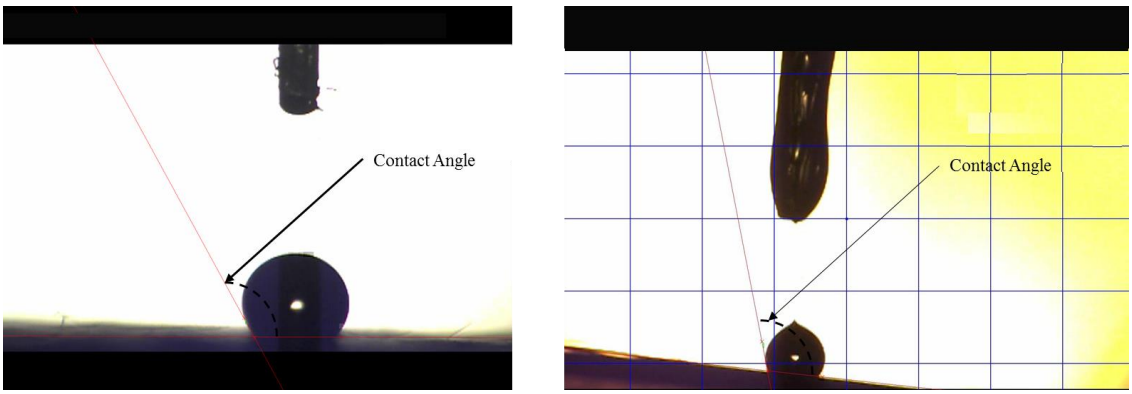

Figure 29 (a) contact angle measurement for B24 Carbon fiber, (b) contact angle measurement for K30-HTC Carbon fiber

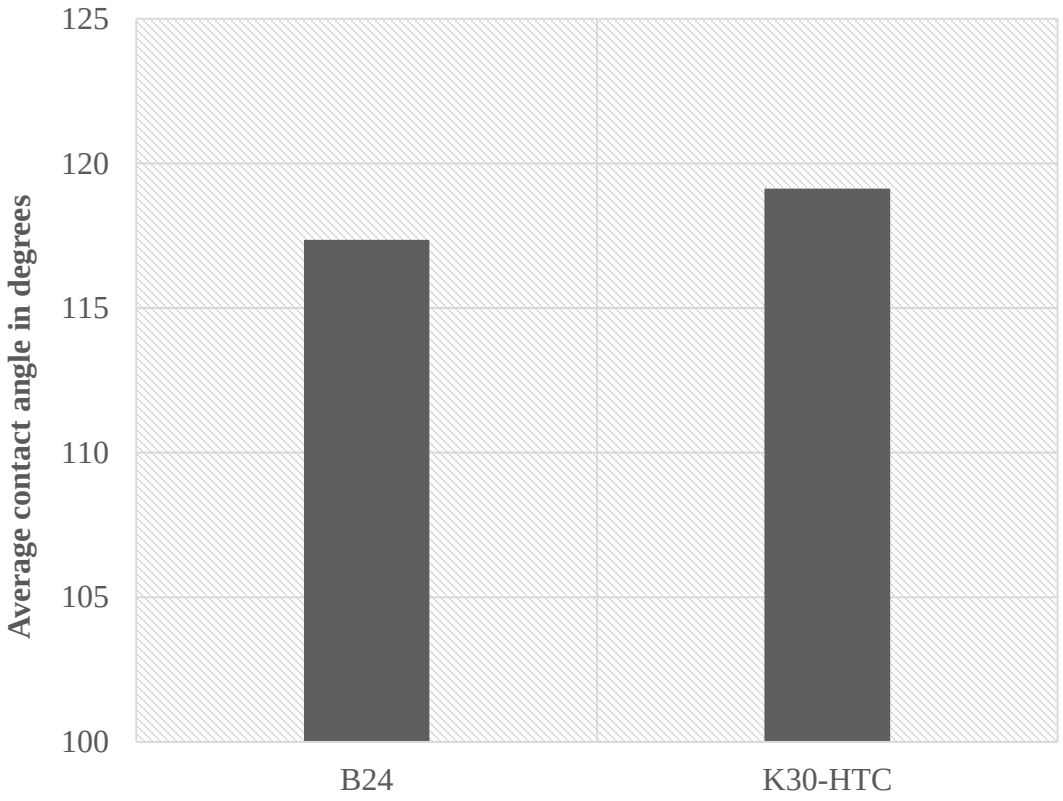

Figure 30 Contact angles for carbon fibers using Vinyl ester as the wetting liquid calculated using Goniometer

4.8 X-ray photoelectron spectroscopy on Carbon fiber surface

Photoemission measurements were performed in a load-locked Kratos XSAM 800 surface analysis system equipped with a hemispherical energy analyzer. The base pressure of this ion- and turbo-pumped system was 8 x 10^{-9} Torr as read on a nude ion gauge. The XPS analyzer was a 127 mm radius double-focusing concentric hemispherical energy analyzer (CHA) equipped with an aberration compensated input lens (ACIL). XPS spectra were recorded in the fixed analyzer transmission (FAT) mode with a pass energy of 80 eV, appropriate for acquisition of medium resolution, high signal-to-noise spectra. The magnification of the analyzer in the FAT mode was selected to collect electrons from the smallest allowable (2 mm^2) area on the specimen. The resolution of the instrument at the operating parameters was measured from FWHM of the $Ag3d_{5/2}$ peak to be 1.0 eV. The XPS energy scale was calibrated by setting the $Ag3d_{5/2}$ line on clean silver to exactly 368.3 eV referenced to the Fermi level. Due to specimen charging during X-ray irradiation, the energy axis of each XPS spectra was shifted to make the C1s binding energy line equal to 285.0 eV, which is a standard hydrocarbon energy (C-H and C-C bonds) used to reference charge affected materials [5, 32, 73, 84]. The photoelectrons were excited by a water-cooled, conventional (i.e., non-monochromatic) dual anode X-ray gun equipped with an Al window. The angle of the incidence of the x-ray beam with the specimen normal was 51.5°. MgKα (1253.6 eV) radiation was used exclusively. The Savitzky-Golay [85] smoothing routine was used in order to help determine the peak binding energies and reduce the noise in the spectra. The XPS surface composition was calculated based on the Scofield cross-sectional values [86] accounting for the instrumental transmission function in the FAT mode of operation.

XPS is a true surface technique, allowing detection of all elements of the period table (except H) located within the first 50 Å of the analyzed surface to a sensitivity of ~ 0.01 atom % (parts per hundred thousand, volumetrically). XPS provides an area-averaged analysis over roughly a 2 mm x 2 mm area on the surface.

Three C fiber specimens were supplied, labeled B-12, K-15U, and Mitsubishi. These specimens were then mounted into the AES/XPS system by double-sided C tape with no additional pretreatment or special handling. The thickness of the fibers was sufficient to completely cover the tape so there would be no XPS signal from it. The analysis protocol consisted of the following procedure, applied to each specimen.

- An "as received" XPS survey spectrum showing all the elements.
- High-resolution spectra of O1s and C1s peaks, plotted using specialty XPS software and compared to common peak positions for various compounds.

The spectra were recorded near the center of a densely populated portion of the fibers. Each spectrum displayed was mathematically smoothed after acquisition using the Savitzky-Golay algorithm (11-pt).

Figure 31a-c shows typical XPS survey scan for three of the carbon fiber samples. The carbon fiber surface is composed of carbon, oxygen & nitrogen. A trace amount of sulfur has been reported by Dilsiz et al [84] and Y. Lou et al [73] in their analysis of carbon fiber surfaces, a similar observation was not made during this study. As expected for typical carbon fiber surfaces, carbon was the main component followed by oxygen and a small percentage of nitrogen was also observed. Table 7 shows the percentage of each component on the carbon fiber surfaces. Furthermore, high resolution spectra of C1s (Figure 32a-c) was fit to Gaussian function to study the functional groups involved. It

was observed that sample K-15U was decidedly different from the other two in that the C1s peak was very wide by comparison. Wide peaks in XPS usually mean there are more chemical subgroups in the specimen than compared to specimens with narrow peaks, which translates to more chemical subgroups and more sub-peaks to make up the wide C1s peak.

Table 7 XPS surface composition of carbon fiber samples

Samples	C1s		O1s		N1s	
	BE(eV)	AC (%)	BE (eV)	AC (%)	BE(eV)	AC (%)
Mitsubishi	285.0	77.2	532.6	22.2	400.9	0.6
K-15U	285.0	77.1	532.6	20.9	400.9	2.0
B12	285.0	80.4	532.6	16.6	400.9	3.0

Further analysis to assign functional groups on C1s was conducted on the basis of literature to understand different chemical shifts in the organic compounds [32, 73, 84, 87, 88]. The percentage of various functional groups were estimated from the curve fit and are summarized in Table 8. The high atomic concentration (AC) of C1s for B12 explains the high roughness and Young's modulus values reported in previous sections. It was also observed that B12 carbon fibers had large amount of functional groups containing oxygen (36.6% and 7.5%) It is widely believed that functional groups having oxygen are acidic and therefor they have better adhesion with epoxy since the polar component of epoxy resin is basic [73, 84]. The lower percentage of C-OH & C=O in Mitsubishi fibers can also be due to a different surface treatment for these fibers as compared to B12 & K-15U fibers supplied by ORNL.

Table 7 XPS carbon 1s curve fit results of carbon fiber samples

Samples	C1s							
	1		2		3		4	
	BE(eV)	AC (%)	BE (eV)	AC (%)	BE(eV)	AC (%)	BE(eV)	AC (%)
Mitsubishi	285.0	74.4	286.1	21.2	288.5	4.4	289.8	0.1
K-15U	285.0	64.9	286.1	28.1	288.5	6.9	289.8	0.1
B12	285.0	55.8	286.1	36.6	288.5	7.5	289.8	0.1
Peak Assignment	C-C & C-H		C-OH, C-OR, C=N		C=O		COOH & COOR	

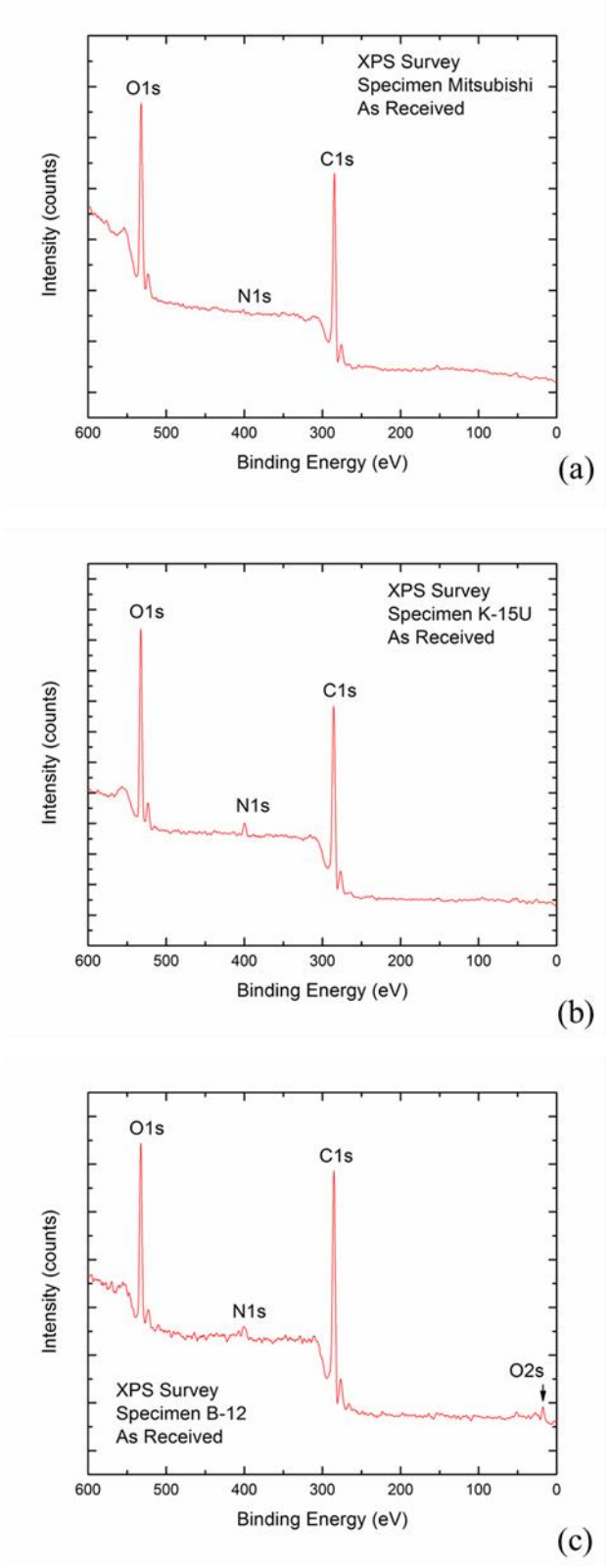

Figure 31 XPS survey scans for (a) Mitsubishi. (b) K-15U and (c) B-12 carbon fibers

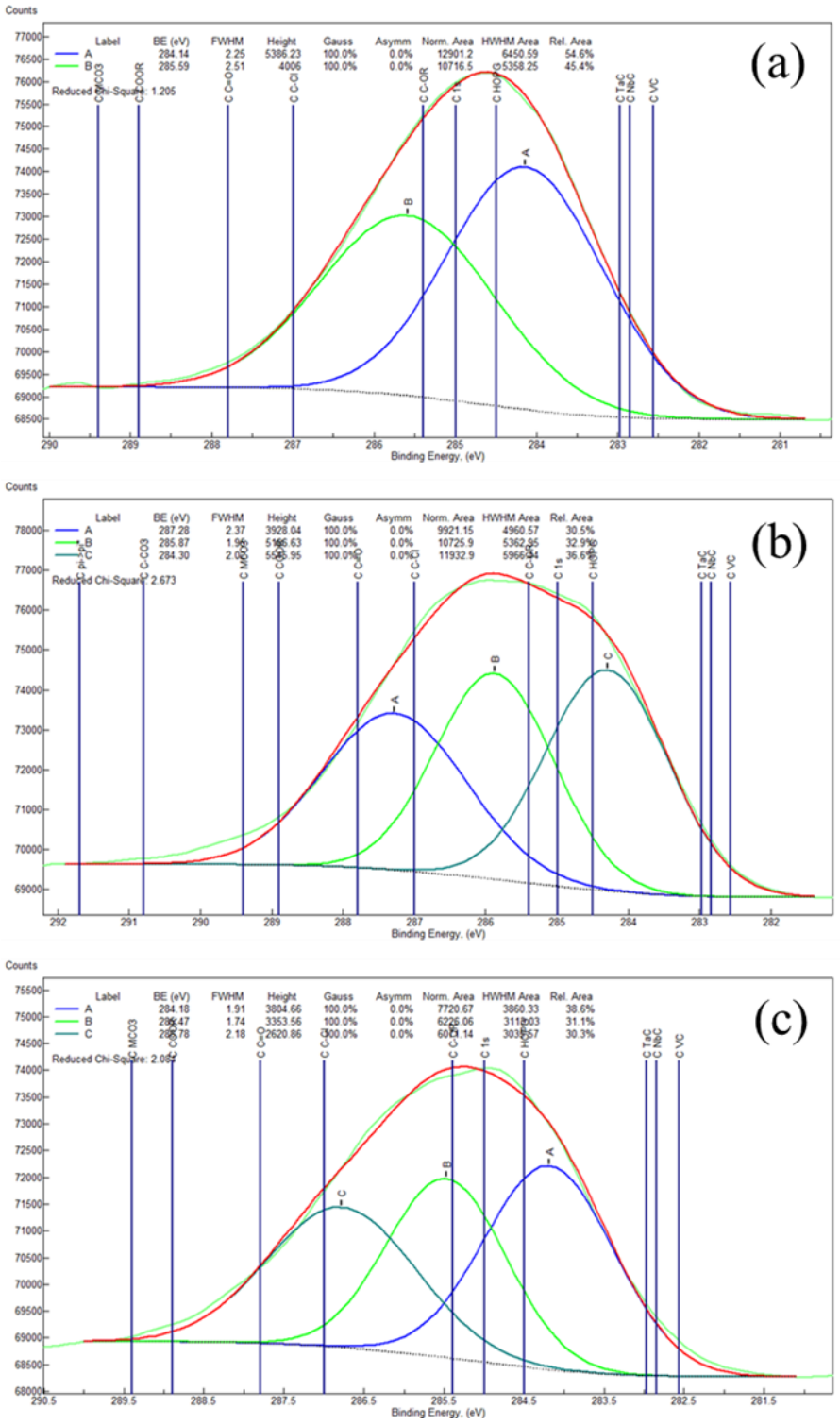

Figure 32 Curve fit of carbon 1s photoelectron peaks of (a) Mitsubishi. (b) K-15U and (c) B-12 carbon fibers

5. CONCLUSION

This study addresses the interfacial characteristics in fiber reinforced composites. Finite element models were developed to study the interfacial behavior during pull out of a single fiber in continuous fiber reinforced polymer composites. 3-D unit cell models using cohesive damage modeling for fiber/matrix interface debonding were employed to investigate effect of interface/sizing coverage on the fiber. Furthermore 2-D axi-symmetric model was also used in a parametric study to analyze sensitivity of interface stiffness, interface strength, friction coefficient, and fiber length. A third 2-D axi-symmetric model was used to study the shear stress distribution across the fiber-interface-matrix zone. These models have shown good potential to predict the load-displacement behavior. However, the finite element models need to be validated by comparing with experimental test results. With the availability of large data sets from experimental test results, our finite element models can be improved upon to predict load displacement interfacial behavior during a fiber pull out. Having analyzed the fiber/matrix interface using both 3-D models and 2-D models, it is clear that both the approaches have their advantages over one another, however the 2-D axi-symmetric model with its relatively simple & user friendly approach coupled with lesser computational time should be preferred. Since both the models (3-D and 2-D) follow the same principles of Cohesive Zone Modeling there is not much of a difference between the fundamentals applied

Surface characterization of carbon fibers was also conducted to better understand the effect of different chemical groups and physical behavior of the fiber surfaces. The techniques used were atomic force microscopy, Fourier transform infrared spectroscopy, X-ray photoelectroscopy and contact angle was also measured using a goniometer Using AFM, Young's modulus and hardness for the fiber surface was calculated using force distance spectroscopy. Topography of the fiber surfaces were studied to calculate the roughness for each of the fibers. Furthermore, SEM images were taken to compliment the AFM images and validate the topography. A combination of all these surface techniques revealed the difference in properties of these fibers and both physical and chemical contributions were accounted.

This thesis is divided in two objectives and the associated findings for each objective are as given below.

Objective I: Computational modeling to study the interfacial behavior of single fiber pulled out from a matrix encasing

- The first 3-D model using cohesive law was successfully employed to understand the difference in continuous bonding and discontinuous bonding between the fiber and the matrix. It was observed that the force required to pull out a fiber from the matrix with continuous bond was three times higher than the one with discontinuous bond.
- A parametric study was undertaken to understand the most effective parameters influencing the bonding of the fiber and the matrix. It was observed that cohesive strength of the interface was the most influential parameter. The parameter; cohesive stiffness was not that influential, coefficient of friction played a role only when the

fiber was debonded and effect of fiber embedded length also did not affect the bonding strength to a large extent.

- A 2-D model was developed where the interface was modelled as a separate entity and was bonded to both the fiber and the matrix. This model was also based on cohesive laws. It was observed that the interface debonded from the fiber side and the stresses were gradually transferred to the matrix.

Objective II Surface characterization of carbon fiber to measure the roughness, mechanical properties and chemical compositions

- Surface characterization revealed that Bluestar carbon fibers were rougher and were also stiffer. The AFM results indicated that roughness values were different due to striations on the carbon fiber and this was attributed to different precursor used by the manufacturer. Particularly B12 carbon fiber had the highest roughness and mechanical properties.
- The sizing layer on each of these fibers were similar, this was validated by the use of Fourier transform infrared spectroscopy and X-ray Photoelctroscopy. Both the test results showed similar chemical constituents. The better roughness values for B-12 fibers was due to higher percentage of carbon more specifically due to presence of C-OH and C-N.
- The roughness values were also complimented with wettability studies which revealed a lower contact angle for Kaltex fibers. This validated our hypothesis that higher roughness would lead to better bonding or wettability

6. RECOMENDATION FOR FUTURE WORK

The results obtained through this research present numerous capabilities in determining the interfacial characteristics of both Carbon fiber and Glass fiber. Following is a list of recommendations for future work in this area.

- Unit cell modelling incorporating roughness parameters obtained from AFM in DIGIMAT-FE or other similar micromechanical modelling suites.
- Mechanical tests to characterize the interface at the macro level in composites and correlate the effects of roughness and other parameters studied at micro level.
- Further elemental analysis to study the effect of each constituent on final properties of carbon & glass fiber reinforced composites
- Surface characterization of sized and unsized fibers to understand the effect of sizing.

7. LIST OF REFERENCES

1. Drzal, L.T., M.J. Rich, and P.F. Lloyd, *Adhesion of Graphite Fibers to Epoxy Matrices: I. The Role of Fiber Surface Treatment.* The Journal of Adhesion, 1983. **16**(1): p. 1-30.

2. Sockalingam, S. and G. Nilakantan, *Fiber-Matrix Interface Characterization through the Microbond Test.* International Journal of Aeronautical and Space Sciences, 2012. **13**(3): p. 282-295.

3. Mason, K., *Sizing up fiber sizings.* URL: http://www.compositesworld.com/articles/sizing-up-fiber-sizings. [cited 06 Sep 2012], 2006.

4. Thomason, J.L. and L.J. Adzima, *Sizing up the interphase: an insider's guide to the science of sizing.* Composites Part A: Applied Science and Manufacturing, 2001. **32**(3–4): p. 313-321.

5. Nursel Dilsiz, J.P.W., *Effect of acid-base properties of unsized and sized carbon fibers on fiber epoxy/matrix adhesion.* Colloids and Surfaces, 1999. **164**(2000): p. 325-336.

6. Drzal, L.T., *Fiber, matrix, and interface properties*. Vol. 1290. 1996: ASTM International.

7. Dey, M., et al., *Influence of sizing formulations on glass/epoxy interphase properties.* Composites Part A: Applied Science and Manufacturing, 2014. **63**: p. 59-67.

8. Drzal, L., *The interphase in epoxy composites*, in *Epoxy Resins and Composites II*, K. Dušek, Editor. 1986, Springer Berlin Heidelberg. p. 1-32.

9. Pitkethly, M.J., et al., *A round-robin programme on interfacial test methods.* Composites Science and Technology, 1993. **48**(1–4): p. 205-214.

10. Gaur, U. and B. Miller, *Microbond method for determination of the shear strength of a fiber/resin interface: evaluation of experimental parameters.* Composites science and technology, 1989. **34**(1): p. 35-51.

11. Mallick, P.K., *Fiber-reinforced composites: materials, manufacturing, and design*. 2010: CRC press.

12. Gao, S.-L., E. Mäder, and S.F. Zhandarov, *Carbon fibers and composites with epoxy resins: Topography, fractography and interphases.* Carbon, 2004. **42**(3): p. 515-529.

13. Mäder, E., S.-L. Gao, and J.-K. Kim, *New Nano-Scale Characterization Techniques for Interphases*, in *Interface Controlled Materials*. 2000, Wiley-VCH Verlag GmbH & Co. KGaA. p. 237-242.

14. Corporation, P.S., *XEI Software manual Version 1.8.0*. 2011.

15. Abhilash, V., *Probing the nanoscale interaction forces and elastic properties of organic and inorganic materials using force-distance (F-D) spectroscopy*, in *Department of Mechanical, materials and aerospace engineering*. 2010, University of Central Florida: Orlando, Florida.

16. Dimitriadis, E.K., et al., *Determination of elastic moduli of thin layers of soft material using the atomic force microscope.* Biophysical Journal, 2002. **82**(5): p. 2798-2810.

17. Cordes, R.D. and I.M. Daniel, *Determination of interfacial properties from observations of progressive fiber debonding and pullout.* Composites Engineering, 1995. **5**(6): p. 633-648.

18. Cech, V., E. Palesch, and J. Lukes, *The glass fiber–polymer matrix interface/interphase characterized by nanoscale imaging techniques.* Composites Science and Technology, 2013. **83**(0): p. 22-26.

19. Ikuta, N., et al., *Investigation on resin interphase produced near silane-treated glass fiber in vinyl ester resin.* Composite Interfaces, 2000. **7**(5): p. 511-515.

20. Hodzic, A., Z.H. Stachurski, and J.K. Kim, *Nano-indentation of polymer–glass interfaces Part I. Experimental and mechanical analysis.* Polymer, 2000. **41**(18): p. 6895-6905.

21. Kim, J.-K., M.-L. Sham, and J. Wu, *Nanoscale characterisation of interphase in silane treated glass fibre composites.* Composites Part A: Applied Science and Manufacturing, 2001. **32**(5): p. 607-618.

22. Utracki, L. and B. Favis, *Polymer alloys and blends*. Vol. 4. 1989: Marcel Dekker: New York.

23. Thomason, J.L., *The interface region in glass fibre-reinforced epoxy resin composites: 1. Sample preparation, void content and interfacial strength.* Composites, 1995. **26**(7): p. 467-475.

24. Mäder, E., et al., *Influence of an optimized interphase on the properties of polypropylene/glass fibre composites.* Composites Part A: Applied Science and Manufacturing, 1996. **27**(9): p. 907-912.

25. Eilerman, G.E. and R.L. Kolek, *Method of sizing glass fibers and epoxy resin emulsion therefor*. 1966, Google Patents.

26. Girgis, M.M., *Non-starch containing aqueous sizing composition for glass fibers and sized glass fibers for use in reinforcing elastomers*. 1983, Google Patents.

27. Motsinger, D.L., *Glass fiber sizing composition*. 1977, Google Patents.

28. Scholtens, B.J. and J.C. Brackman, *Influence of the film former on fibre-matrix adhesion and mechanical properties of glass-fibre reinforced thermoplastics.* The Journal of Adhesion, 1995. **52**(1-4): p. 115-129.

29. Gao, X., et al., *Effect of colloidal silica on the strength and energy absorption of glass fiber/epoxy interphases.* Composites Part A: Applied Science and Manufacturing, 2011. **42**(11): p. 1738-1747.

30. Zoltek Companies, I. *What is Carbon Fiber?* 2014; Available from: http://www.zoltek.com/carbonfiber/.

31. GmbH, T.T.E.; Available from: http://www.tohotenax-eu.com/en/products/whats-carbon-fiber/manufacturing-process.html.

32. Morita, K., et al., *Characterization of commercially available PAN (polyacrylonitri1e)-based carbon fibers.* Pure and Applied Chemistry, 1986. **58**(3): p. 455-468.

33. Bascom, W. and L. Drzal, *The Surface Properties of Carbon Fibers and Their Adhesion to Organic Polymers*. 1987, DTIC Document.

34. Sherwood, P.M.A., *Surface analysis of carbon and carbon fibers for composites.* Journal of Electron Spectroscopy and Related Phenomena, 1996. **81**(3): p. 319-342.

35. Gaol, F.L. and F.E. Gunawan, *A New Approach for Debonding Characterization.* EPJ Web of Conferences, 2014. **68**: p. 00034.

36. Chawla, K.K., *Composite materials: science and engineering*. 2012: Springer Science & Business Media.

37. Thower, P.A., & Radovic, L.R, *Chemistry and Physics of Carbon: a series of advances*. 1999, New York: Marcel Dekker.

38. Dai, Z., et al., *Effect of sizing on carbon fiber surface properties and fibers/epoxy interfacial adhesion.* Applied Surface Science, 2011. **257**(15): p. 6980-6985.

39. Cao, X., Wen, Y. -., Zhang, S.-., & Yang, Y.-. *Heat-resistant emulsifying sizing agent for carbon fibers.* New Carbon Materials, 2006. **4**(2006): p. 337-342.

40. O'Brien, J.P., *Handbook of fiber science and technology: Volume 111, high technology fibers, part a, M. Lewin and J. Preston, Eds., Marcel Dekker, New York, 1985, 397 pp.* Journal of Polymer Science Part C: Polymer Letters, 1987. **25**(1): p. 51-51.

41. Donnet JB, B.R., *Carbon fibers, 2nd edition by J. B. Donnet and R. C. Bansal, Marcel Dekker, New York (1990), ISBN 470 pp., .* Polymers for Advanced Technologies, 1992. **3**(1): p. 47-47.

42. Bogoeva-Gaceva, G., et al., *Characterization of the surface and interphase of plasma-treated HM carbon fibres.* Composites Part A: Applied Science and Manufacturing, 1997. **28**(5): p. 445-452.

43. Ochoa-Putman, C. and U.K. Vaidya, *Mechanisms of interfacial adhesion in metal–polymer composites – Effect of chemical treatment.* Composites Part A: Applied Science and Manufacturing, 2011. **42**(8): p. 906-915.

44. Gao, S. and Y. Zeng, *Surface modification of ultrahigh molecular weight polyethylene fibers by plasma treatment. I. Improving surface adhesion.* Journal of Applied Polymer Science, 1993. **47**(11): p. 2065-2071.

45. Hsueh, C.-H., *Interfacial debonding and fiber pull-out stresses of fiber-reinforced composites.* Materials Science and Engineering: A, 1990. **123**(1): p. 1-11.

46. Stang, H. and S.P. Shah, *Failure of fibre-reinforced composites by pull-out fracture.* Journal of Materials Science, 1986. **21**(3): p. 953-957.

47. Gao, Y.-C., Y.-W. Mai, and B. Cotterell, *Fracture of fiber-reinforced materials.* Zeitschrift für angewandte Mathematik und Physik ZAMP, 1988. **39**(4): p. 550-572.

48. Sun, W. and F. Lin, *Computer modeling and FEA simulation for composite single fiber pull-out.* Journal of Thermoplastic Composite Materials, 2001. **14**(4): p. 327-343.

49. Wei, G.F., et al. *Finite element simulation of perfect bonding for single fiber pull-out test*. in *Advanced Materials Research*. 2012. Trans Tech Publ.

50. Dugdale, D.S., *Yielding of steel sheets containing slits.* Journal of the Mechanics and Physics of Solids, 1960. **8**(2): p. 100-104.

51. Barenblatt, G.I., *The Mathematical Theory of Equilibrium Cracks in Brittle Fracture*, in *Advances in Applied Mechanics*, T.v.K.G.K.F.H.v.d.D. H.L. Dryden and L. Howarth, Editors. 1962, Elsevier. p. 55-129.

52. Chandra, N., *Evaluation of interfacial fracture toughness using cohesive zone model.* Composites Part A: Applied Science and Manufacturing, 2002. **33**(10): p. 1433-1447.

53. Hibbit, Karlsson, and Sorensen, *ABAQUS/Standard Analysis User's Manual*. 2007: Hibbit, Karlsson, Sorensen Inc.

54. Cornec, A., I. Scheider, and K.-H. Schwalbe, *On the practical application of the cohesive model.* Engineering Fracture Mechanics, 2003. **70**(14): p. 1963-1987.

55. Quate, C., *The AFM as a tool for surface imaging.* Surface Science, 1994. **299**: p. 980-995.

56. Battleson, K.A., *Surface characterization of pan-based carbon fibers using XPS, SIMS, and AFM*. 1998, Montana State University--Bozeman.

57. Scanners, P. and H.T. Work, *Training Notebook.* 2000.

58. Rath, S.K., et al., *Two component silicone modified epoxy foul release coatings: Effect of modulus, surface energy and surface restructuring on pseudobarnacle and macrofouling behavior.* Applied Surface Science, 2010. **256**(8): p. 2440-2446.

59. Wang, Y. and T.H. Hahn, *AFM characterization of the interfacial properties of carbon fiber reinforced polymer composites subjected to hygrothermal treatments.* Composites Science and Technology, 2007. **67**(1): p. 92-101.

60. Chen, X., et al., *Phase contrast and attraction–repulsion transition in tapping mode atomic force microscopy.* Surface Science, 2002. **519**(1–2): p. L593-L598.

61. Kumar, G.K., *Studying the influence of glass fiber sizing roughness and thickness with the single fiber fragmentation test.* Kristianstad University, Degree Project, 2006.

62. Firehole Technologies, I., *Helius: MCT Tutorial 1*. 2011.

63. Bheemreddy, V., et al., *Modeling of fiber pull-out in continuous fiber reinforced ceramic composites using finite element method and artificial neural networks.* Computational Materials Science, 2013. **79**: p. 663-673.

64. Scheer, R. and J. Nairn, *A comparison of several fracture mechanics methods for measuring interfacial toughness with microbond tests.* The Journal of Adhesion, 1995. **53**(1-2): p. 45-68.

65. Sockalingam, S., et al., *Finite element analysis of the microdroplet test method using cohesive zone model of the fiber/matrix interface.* Composites Part A: Applied Science and Manufacturing, 2014. **56**: p. 239-247.

66. Jia, Y., W. Yan, and H.-Y. Liu. *Numerical study on carbon fibre pullout using a cohesive zone model*. in *18th International Conference on Composite Materials, Jeju Island, Korea*. 2011.

67. Gao, S.-L. and E. Mäder, *Characterisation of interphase nanoscale property variations in glass fibre reinforced polypropylene and epoxy resin composites.* Composites Part A: Applied Science and Manufacturing, 2002. **33**(4): p. 559-576.

68. Mai, K., E. Mäder, and M. Mühle, *Interphase characterization in composites with new non-destructive methods.* Composites Part A: Applied Science and Manufacturing, 1998. **29**(9–10): p. 1111-1119.

69. Oliver, W.C. and G.M. Pharr, *Measurement of hardness and elastic modulus by instrumented indentation: Advances in understanding and refinements to methodology.* Journal of materials research, 2004. **19**(01): p. 3-20.

70. Dong, C. and I.J. Davies, *Flexural properties of E glass and TR50S carbon fiber reinforced epoxy hybrid composites.* Journal of materials engineering and performance, 2013. **22**(1): p. 41-49.

71. León, C.A.L., *Carbon Fibers Having Improved Strength And Modulus And An Associated Method And Apparatus For Preparing Same*. 2015, Google Patents.

72. Choi, H., et al., *Review paper: Toward highly efficient quantum-dot-and dye-sensitized solar cells.* Current Applied Physics, 2013. **13**: p. S2-S13.

73. Luo, Y., et al., *Surface and wettability property analysis of CCF300 carbon fibers with different sizing or without sizing.* Materials & Design, 2011. **32**(2): p. 941-946.

74. Scott, W.W. and B. Bhushan, *Use of phase imaging in atomic force microscopy for measurement of viscoelastic contrast in polymer nanocomposites and molecularly thick lubricant films.* Ultramicroscopy, 2003. **97**(1–4): p. 151-169.

75. Krekel, G., K.J. Hüttinger, and W.P. Hoffman, *The relevance of the surface structure and surface chemistry of carbon fibres in their adhesion to high temperature thermoplastics.* Journal of Materials Science, 1994. **29**(13): p. 3461-3468.

76. Heinz, W.F. and J.H. Hoh, *Spatially resolved force spectroscopy of biological surfaces using the atomic force microscope.* Trends in biotechnology, 1999. **17**(4): p. 143-150.

77. Donnet, J.-B., *Carbon fibers*. 1998: CRC Press.

78. Chatzi, E., et al., *Determination of the accessibility of N・H groups of Kevlar 49 fibres by photoacoustic FTi. r. spectroscopy.* Polymer, 1986. **27**(12): p. 1850-1854.

79. Wang, S. and A. Garton, *Chemical interactions at the interface between a carbon fiber and a boron trifluoride-catalyzed epoxy matrix.* Journal of applied polymer science, 1992. **45**(10): p. 1743-1752.

80. Cole, K., et al., *Comparison of infrared spectroscopic methods for the quantitative analysis of epoxy resins used in carbon-epoxy composite materials.* Applied spectroscopy, 1988. **42**(5): p. 761-769.

81. Sellitti, C., J. Koenig, and H. Ishida, *Surface characterization of graphitized carbon fibers by attenuated total reflection Fourier transform infrared spectroscopy.* Carbon, 1990. **28**(1): p. 221-228.

82. Jones, C., *The chemistry of carbon fibre surfaces and its effect on interfacial phenomena in fibre/epoxy composites.* Composites Science and Technology, 1991. **42**(1–3): p. 275-298.

83. Yuan, Y. and T.R. Lee, *Contact Angle and Wetting Properties*, in *Surface Science Techniques*, G. Bracco and B. Holst, Editors. 2013, Springer Berlin Heidelberg. p. 3-34.

84. Dilsiz, N. and J. Wightman, *Surface analysis of unsized and sized carbon fibers.* Carbon, 1999. **37**(7): p. 1105-1114.

85. Savitzky, A. and M.J. Golay, *Smoothing and differentiation of data by simplified least squares procedures.* Analytical chemistry, 1964. **36**(8): p. 1627-1639.

86. Scofield, J., *Lawrence Livermore Laboratory Report No.* UCRL-51326, 1973.

87. Drzal, L.T., et al., *Adhesion of Graphite Fibers to Epoxy Matrices: II. The Effect of Fiber Finish.* The Journal of Adhesion, 1983. **16**(2): p. 133-152.

88. Smiley, R.J. and W.N. Delgass, *AFM, SEM and XPS characterization of PAN-based carbon fibres etched in oxygen plasmas.* Journal of Materials Science, 1993. **28**(13): p. 3601-3611.